LTV Missiles and Electronics Group
Missiles Division

(4)

Contract Report N00014-87-C-0114

A Nonlinear-Optical Method for Combining High Power Laser Beams

28 April 1989

(4)

LTV MISSILES AND ELECTRONICS GROUP
MISSILES DIVISION

Report No. 3-45400/9R-57

Contract Report N00014-87-C-0114

A Nonlinear-Optical Method for Combining High Power Laser Beams

28 April 1989

Jay S. Chivian, C. A. Glosson, W. D. Cotten,
C. D. Cantrell, III, S. F. DiMarco, and S. T. Garner

Prepared for:

Office of Naval Research
495 Summer Street
Boston, MA 02210-2109
Attn: Dr. Matthew B. White

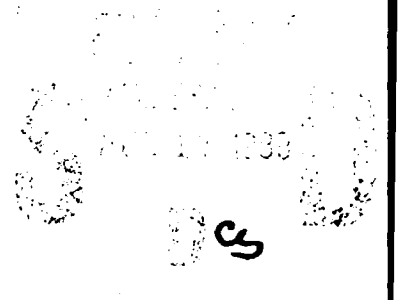

Prepared by:

LTV Missiles and Electronics Group
Missiles Division
P. O. Box 650003
Dallas, TX 75265-0003

Supported by:

Center for Applied Optics
University of Texas at Dallas
P. O. Box 830688
Richardson, TX 75083-0688

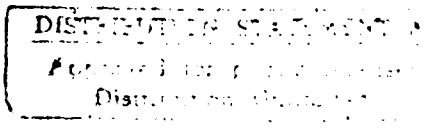

SUMMARY

This report covers the technical effort under Contract No. N00014-87-C-0114 for the period 1 April 1988 to 30 April 1989. The overall program goal was to investigate concepts for laser-controlled optics based on near-resonance nonlinear dispersion in gases, and to demonstrate a laser-induced grating capable of high power laser beam combining. The theoretical work extended the previous year's effort in giving a more detailed view of those aspects which might prevent observation of a grating, and led to optimization of experimental parameters. Modifications and improvements were made to the experimental apparatus. No grating was observed over a wide range of experimental conditions, although the apparatus was capable of such demonstration had a grating existed. The most likely cause of trouble appears to be the complexity of the SF_6 medium chosen for demonstration. As an apparatus check, a medium (e.g., vanadium dioxide) can be used in which it is known that a grating can be demonstrated. Measurements were extended on the effect of noble gas admixtures into SF_6 on the absorption of 16.26 μm radiation; helium suppresses absorption, argon and xenon enhance absorption. It would be worthwhile to continue these studies in light of information to be gained regarding the effect of collisions on absorption spectra in molecular species.

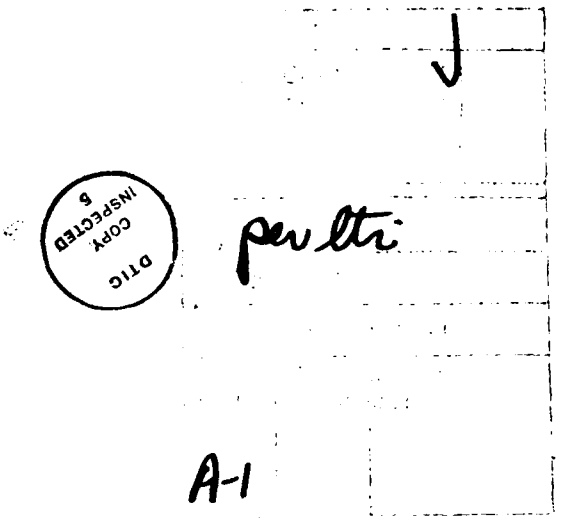

TABLE OF CONTENTS

1.0 INTRODUCTION

1.1 Objective

The objective of this program was to continue investigations of concepts for laser-controlled optics based on near-resonance nonlinear dispersion in gases, so that a laser-induced grating capable of high power laser beam combining might be demonstrated.

1.2 Background

The principle of coherent addition of several input laser beams into one output beam had been demonstrated by the use of binary phase gratings which had been etched onto a solid surface, establishing that multiple laser beams can be combined into a single beam with good conversion efficiency.[1]

For high power beams, the limited damage threshold and maximum permissible thermal loading of solid state devices encouraged a search for more satisfactory working media. Gases and plasmas appeared to offer better solutions as working media; in them convective cooling can be used for thermal dissipation. Coincidentally, it had been predicted that two laser fields of differing wavelengths interacting with a collision-dominated atomic or molecular system with three effective energy levels could influence one another in a nonreciprocal manner; the creation of and interaction with a grating via near-resonance nonlinear dispersion thus should provide a method for low power laser beams to create a grating in which other beams combined to form a high power beam.[2,3]

With these basic concepts in mind, we proposed to investigate the feasibility of using overlapping laser beams to write a grating or thick hologram in the index of refraction of a gas or plasma with a weak beam under such conditions that the grating would not be destroyed by the beams the grating was designed to deflect; to find media in which this could be accomplished for laser wavelengths of interest; and to undertake proof-of-principle and exploratory experiments on promising systems. The first part of the investigation took place from 28 December 1986 to 31 March 1988; a report[4] on that work followed and is summarized briefly below.

The key technical issues to be addressed were: (1) can a grating appropriate for beam combining be made in a gaseous medium, and (2) can high power beams really be controlled by lower power beams using near-resonance nonlinear dispersion as predicted in Reference 2?

The first task performed in the 1987-1988 effort was to select a nonlinear medium suitable for proof-of-principle demonstration. Sulfur hexafluoride (SF_6) was chosen from three candidates because the properties of SF_6 are reasonably well known, and absorption resonances exist near prominent lines of the carbon tetrafluoride (CF_4) laser and the carbon dioxide (CO_2) laser.

An existing computer program was available to evaluate dispersion relations for a three level system, including the effects of saturation, when either the probing or pumping field changed strength or frequency.[5] The code was modified to include dependence on spatially varying incident radiation fields, and the necessary data for SF_6 were input to the code; the output was an index-of-refraction map as seen by the probe field.

The probe beam interaction with the grating was modeled using coupled wave theory,[6] where the grating shape was carried forward from the dispersion calculations. Software was written for single probe beam diffraction by the grating, and for two beam combination.

Gratings were also designed to combine more than two beams, but for the simplest possible system to demonstrate proof-of-principle, a grating created by two pump beams for combining two probe beams was chosen. The original analysis was modeled on uniform amplitude plane waves of infinite extent.

An experimental setup was assembled for proof-of-principle demonstration, the main parts of which were a CF_4 pump laser optically pumped by a CO_2 TEA laser, a pulse-pumped CO_2 probe laser, and a sample or interaction cell for the SF_6. The cell had potassium bromide (KBr) windows separated by 1.57 cm. The sample cell gas manifold provided for operation with pure SF_6 or with admixture of helium buffer gas.

Attempts to demonstrate the presence of a grating created by 16.26 μm beams from the CF_4 laser by diffraction of 10.55 μm radiation from the CO_2 laser in either pure SF_6 or in SF_6 buffered with helium were unsuccessful. Furthermore, it was discovered that the addition of He as a buffer gas suppressed the absorption of 16.26 μm in SF_6.

The following problem areas were identified, and recommendations were made for their resolution. It was felt that the stability of the 16.26 μm pump radiation could be improved by remounting the CO_2 TEA laser which served as the optical pump for the CF_4 laser. The effects of buffer gas on the absorption of 16.26 μm energy in SF_6 needed to be reexamined with fast power detectors (as opposed to an energy meter), and argon and xenon were recommended in addition to helium. Also, with fast detectors, spatial and temporal diagnostics could be carried out on the 16.26 μm beam. Preliminary tests showed that the presence of 10.55 μm radiation did not affect the absorption of 16.26 μm, but further examination was indicated. The temporal displacement between pump and probe radiation in the sample interaction region was also in question because of the substantial differences in pulse widths; a CO_2 TEA laser was recommended for the probe source, if such could be acquired.

With these major thrusts in mind, work began on the next phase, with emphasis on finding answers to unresolved questions.

1.3 Approach

The major factor affecting the path of the investigation was the discovery that the addition of helium to low pressure sulfur hexafluoride suppressed the absorption of 16.26 μm pump radiation. In keeping with the original suggestion that a collision-dominated medium was essential,[2] it would be necessary to raise the SF_6 pressure so that the SF_6 would be <u>self</u> collision-dominated. Then, due to the high specific absorption of the 10.55 μm probe radiation, the sample cell thickness (and therefore the grating thickness) had to be reduced to compensate.

We were thus driven to consider the consequences of the changes to a 1 mm thick sample region, and SF_6 pressure change from the original 0.1 Torr to a nominal 10 Torr. These and other factors are discussed in the following sections.

Technical effort covered the period from 1 April 1988 to 30 April 1989. This report presents the technical discussion and results in section 2, with each proposed task in its own subsection. A conclusions and recommendations section 3 follows. The report ends with a reproduction of the paper given at the SPIE meeting OE/LASE '89 in January 1989 at Los Angeles, CA, in the appendix.

2.0 TECHNICAL DISCUSSION AND RESULTS

2.1 Task 1 - Beam Interaction Analysis

The theoretical effort has attempted to understand and explain the experimental results. A more detailed view was accorded various aspects of the proof-of-principle experiment: the effect of finite beam size, the importance of knowing the precise background index of refraction, the effect of non-monochromaticity, the sensitivity of the absorbing medium to laser frequency, and the sensitivity of the diffraction efficiency to Bragg angle.

Various aspects of the experimental setup were examined to see if any one or some combination of them could be washing out any beam-induced grating. The first of these effects to be addressed was that of using finite sized beams. Since the theory developed from the coupled wave expansion of Gaylord and Moharam[6] required that the input plane waves have infinite extent, there was reason to suspect that using plane waves of finite extent in the transverse dimension would have a considerable effect on the outcome of the experiment. This approximation was examined by enclosing the grating within a Gaussian envelope and integrating to obtain the Fourier coefficients over the entire grating width, not just a single grating period. Integrating over a single grating period is acceptable for beams of infinite extent because all the grating periods are identical. The resulting expressions for the dielectric coefficients are somewhat smaller than those produced for infinite beams, but the differences are less than expected for the effective beam area, defined as that portion of the beam enclosed within the $1/e^2$ power points. Although the effective region of interaction is smaller than the region for the infinite beams, most of the available beam area is still available for use in creating the grating. The net result is that while the overall area in which the grating is produced has decreased, the interaction within that region is roughly the same as the infinite beam case, and hence there should be more diffraction into the higher orders, even though the total amount of diffraction will be smaller than for the ideal case. This does not appear to be a real impediment to observation of a grating, only to the quantity of radiation observed in the higher orders.

...t, the potential effect of calculating the precise background index of refraction was examined. The typical index of refraction for a gas is on the order of 1.01 - 1.0001. A test was conducted in which these indices were used as the background index of refraction, and the results confirmed the notion that the background index of refraction is not important. The results showed that the only real change was in the Bragg angle and that only varied by a few hundredths of a degree, which for the thinner grating cell currently employed in the experiment has no experimentally observable effect. Theoretical calculations show that there will be a decrease in the diffraction efficiency to the higher orders, but only about 1-2 percent. This then does not seem to be a significant contributor to the lack of an observed grating in the cell.

As was mentioned in the SOW, the values of the linear part of the index of refraction were thought to be of some importance to the calculation. Thus it was proposed to calculate these values using a spectral simulation for known constants of SF_6, but when it was shown that the background index of refraction was of minimal importance, these investigations were discarded.

The effect of non-monochromaticity can be extreme. Using beams with infinite transverse extent, the question was asked as to how close together must two different line frequencies be in order to produce a grating with the same size as that produced in the first section by finite sized beams. If the grating was to have a 1 cm radius (the finite beams in the experiment have roughly a radius of 0.6 cm) what must the two frequencies k_1 and k_2 be for the area of first maximum to cover a circle of 1 cm radius? Using k_1 as 945 cm^{-1}, k_2 was calculated to be about 948 cm^{-1} under the condition that the cosines of k*1cm for each of the frequencies were out of phase with each other by π. These frequencies are far enough apart that neighboring lines in the CO_2 laser would be required. This could be a significant problem, but these lines can be easily separated by the use of a proper grating or etalon. There does not appear to be any extra mode present in the CO_2 beam. More problems would be caused by the resulting non-stationary gratings. For a pair of beams each of two distinct frequencies, there will be four gratings produced; two stationary ones which were just discussed, and two non-stationary ones. The non-stationary gratings are much more difficult to gauge, but should average over time to be negligible, if the experimental apparatus is locked to a single output frequency for the pump beams.

The next area for investigation was the sensitivity of the change in the real part of the index of refraction as seen by the 10.55 μm probe radiation to the detuning of the 16.26 μm pump radiation. Figure 2.1.1 displays a graph of the sensitivity of the real index of refraction to the detuning of the CF_4 laser from the absorption edge when the SF_6 pressure is 0.1 Torr, the pressure used in the initial attempts to establish a grating. It is readily apparent that the absorption of the SF_6 at the laser frequency (615.1 cm^{-1}) is much smaller than near the absorption edge (615.0247 cm^{-1}). Indeed, the absorption is a factor of 20 smaller. Lest this graph seem too disturbing, it should be noted that this figure was produced using an absorption line, whereas SF_6 has an absorption band. The fact that the ν_4 band of SF_6 has a very sharp absorption edge would still cause significant difficulty were it not for the fact that the absorption edge is distorted by thermal effects. As a result, it is not possible to determine solely by theoretical means precisely what the absorption is for the laser line of interest. What can be said is that the absorption of the ν_4 band of SF_6 lies between the extremes of maximum absorption and the minimum displayed on the graph.

With the projected change to higher pressure, the sensitivity of the SF_6 system to the frequency offset of the pump laser from the absorption edge was recalculated for 10 Torr; the result is shown in Figure 2.1.2. One notes two substantive changes: (1) at the higher pressure, the percentage real index change is much smaller than at lower pressure, that is, the higher pressure SF_6 is less sensitive to frequency offset, and (2) the magnitude of the real index change at the absorption edge is roughly the same ratio as the pressure, 100 times larger at 10 Torr than at 0.1 Torr. Other considerations (discussed below) led to an predicted optimum operating pressure of 1.5 Torr; calculated sensitivity to frequency offset at 1.5 Torr is shown in Figure 2.1.3. Although it is satisfying that the sensitivity to detuning is predicted to be relatively small at pressures above 1 Torr, caution is indicated because the effect of pressure in possibly frequency-shifting the absorption edge is unknown, and is not accounted for in the model.

The sensitivity of diffraction efficiency to the departure of the incident probe beam angle from the precise value of the Bragg angle is expected to be

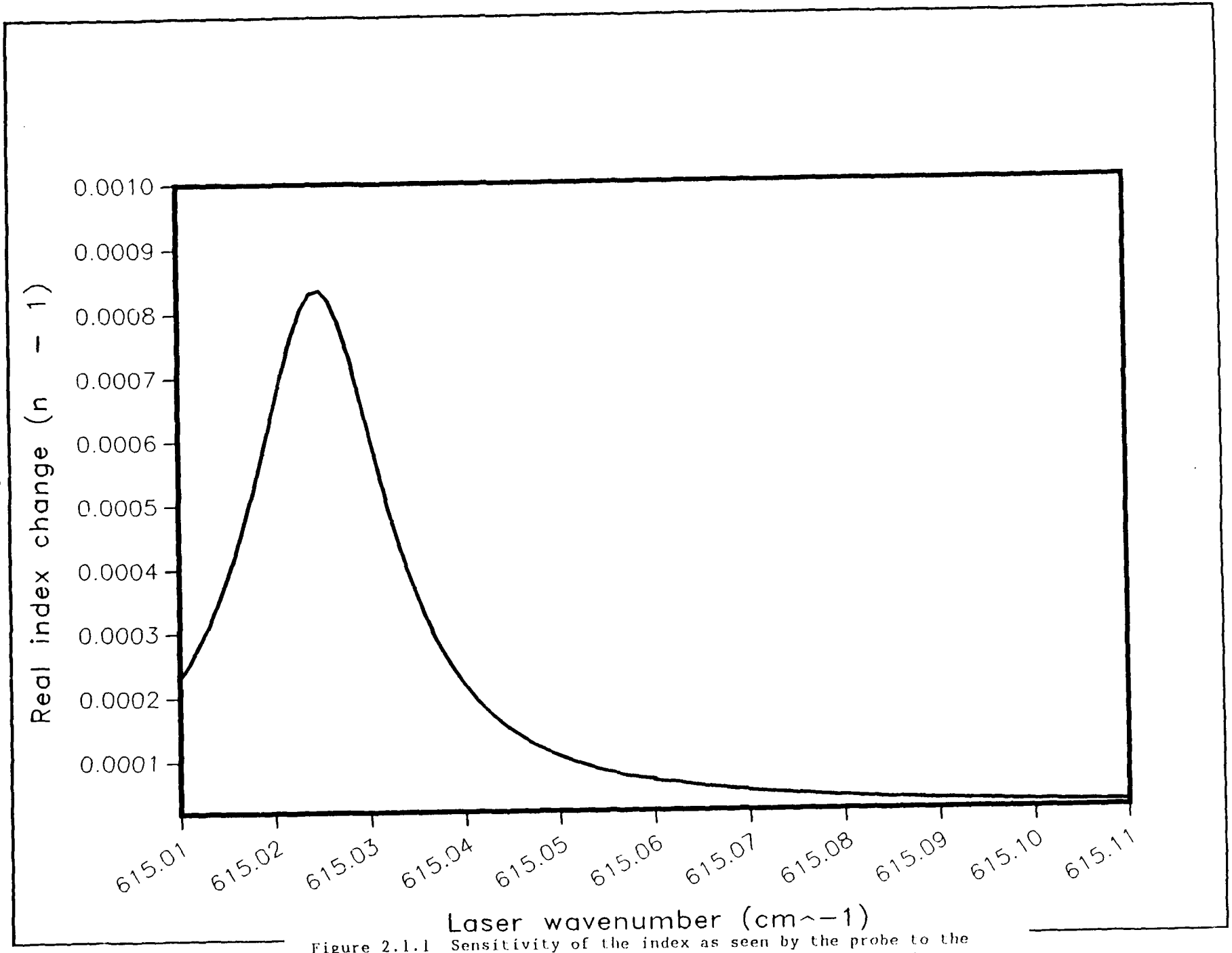

Figure 2.1.1 Sensitivity of the index as seen by the probe to the frequency offset of the pump; SF_6 pressure 0.1 Torr

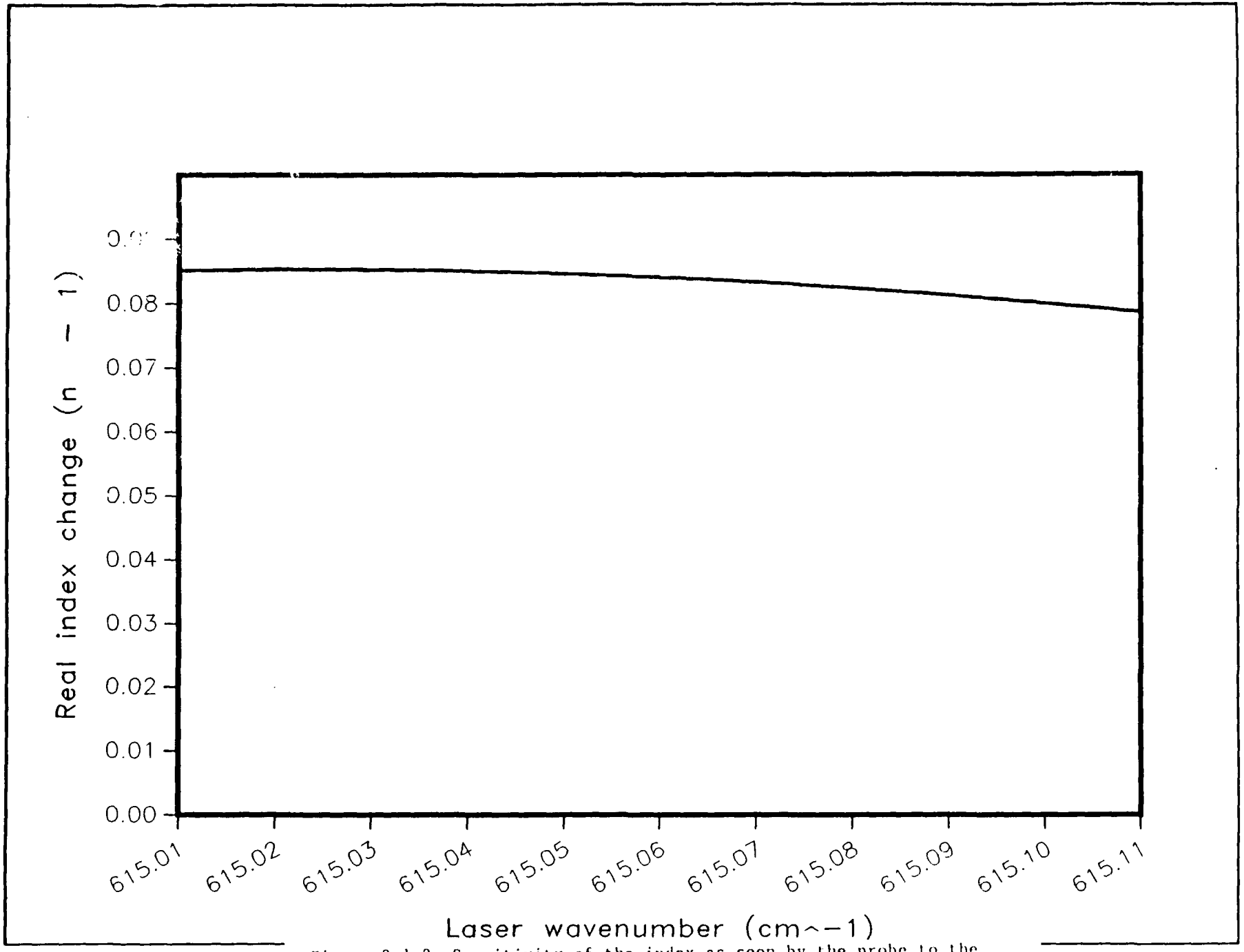

Figure 2.1.2 Sensitivity of the index as seen by the probe to the frequency offset of the pump; SF_6 pressure 10 Torr

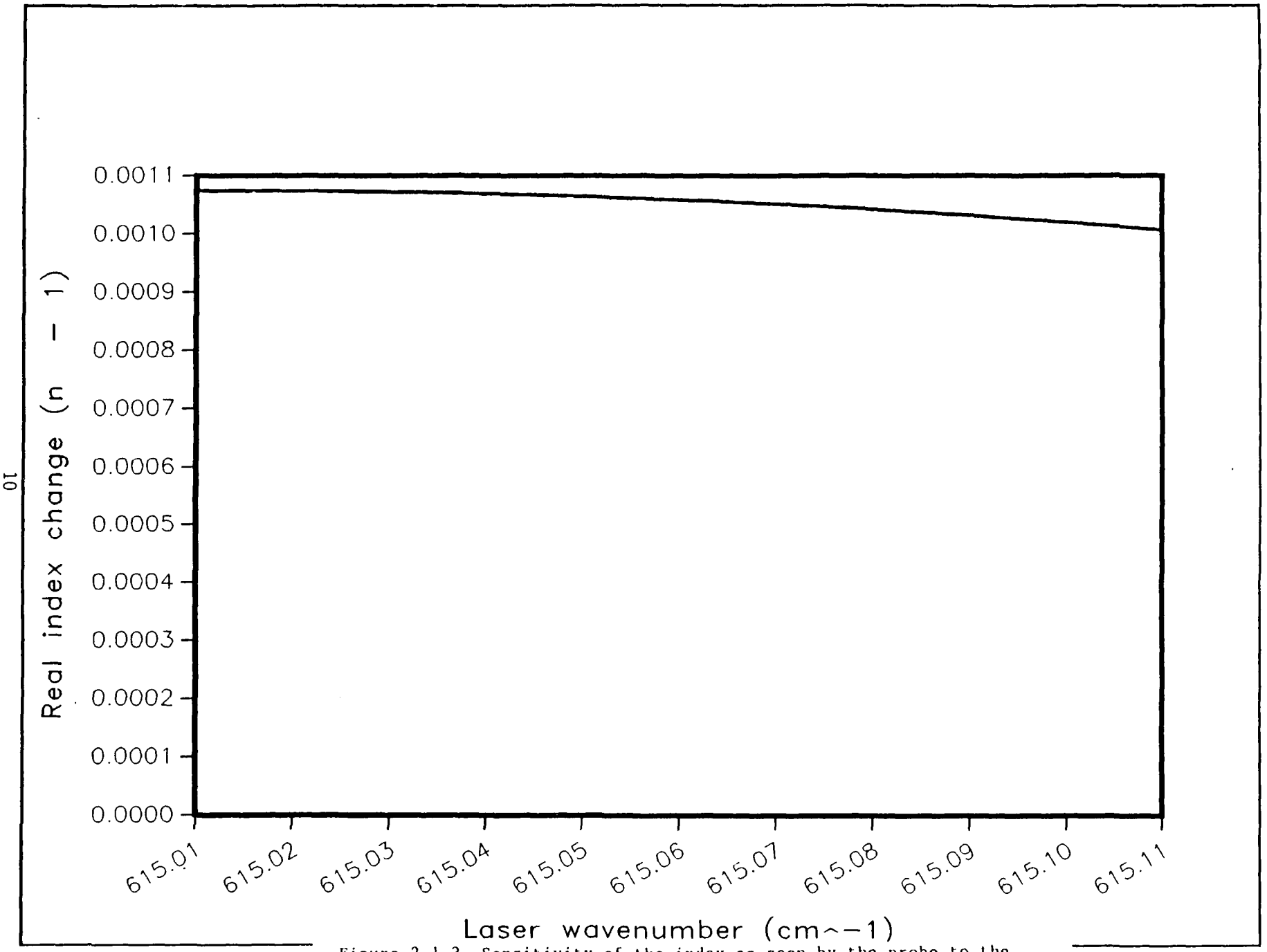

Figure 2.1.3 Sensitivity of the index as seen by the probe to the

influenced by the change of grating thickness from 1.57 cm to 1 mm. Figure 2.1.4 shows the sensitivity of the diffraction efficiency for a grating thickness of 1.57 cm. The curve in Figure 2.1.4 has been calculated for conditions which would optimize beam combining; that is, for two equal intensity input beams each at the exact Bragg angle (+ and -). Thus, at 0 angle off Bragg, the total diffraction efficiency is twice the ordinate scale reading. The remaining power is absorbed; less than a fraction of 1% is diffracted into higher orders. Because of the relationship between grating spacing (16.26 μm), probe wavelength (10.55 μm), and index of refraction ($1 \leq n \leq 1.1$), the only orders other than zero and +1 that propagate are -1 and +2; all others are evanescent. Figure 2.1.4 indicates that diffraction efficiency in the 1.57 cm thick sample cell falls to half its maximum value when the incident beam is about 0.02 degree from the precise Bragg angle. This fact made the original experimental setup very sensitive to correct angular setup.

The sensitivity of diffraction efficiency to angle off Bragg for the 1 mm thick grating is shown in Figure 2.1.5, again for conditions optimized for beam combining, although the grating strength and value of the Bragg angle itself are different. Also shown in Figure 2.1.5 is a diffraction efficiency curve (still in the 1 mm cell) when the conditions have been optimized for maximum diffraction into the +1 order (minimum in zero order) at 1.5 Torr SF_6 pressure. In either of the two curves shown, diffraction efficiency falls to half its maximum value about 0.4 degree off Bragg. It is seen that an additional benefit is gained in changing to the 1 mm thick sample cell, that of much reduced experimental sensitivity to angle setting of the probe beam(s).

As a further result of the inability to demonstrate a laser-induced grating in SF_6 in the initial go-around, coupled with the proposed changes in the experimental setup, we were led to re-examine whether or not we would be adhering to the conditions specified by Reference 2. The basic diagram for near-resonance nonlinear dispersion in SF_6 is shown in Figure 2.1.6. We note that the energy offsets Δ_1 and Δ_2 are each greater than the line widths of either pump or probe laser. Δ_1 and Δ_2 also are larger than the Doppler broadening of the SF_6 absorptions up to and including 10 Torr. These are necessary conditions for satisfying "near-resonance."

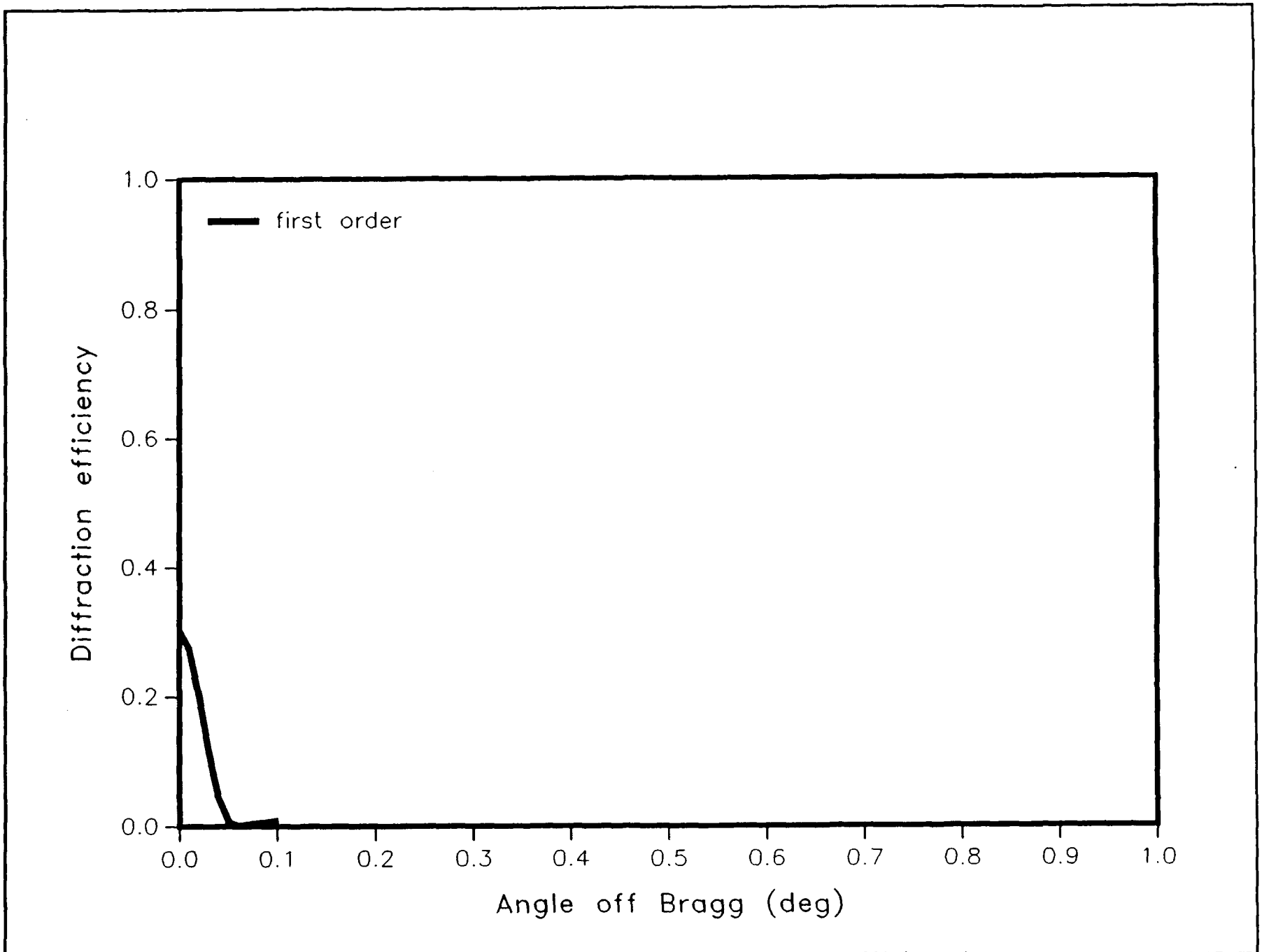

Figure 2.1.4 Sensitivity of first order diffraction efficiency to departures from Bragg angle; grating thickness 1.57 cm

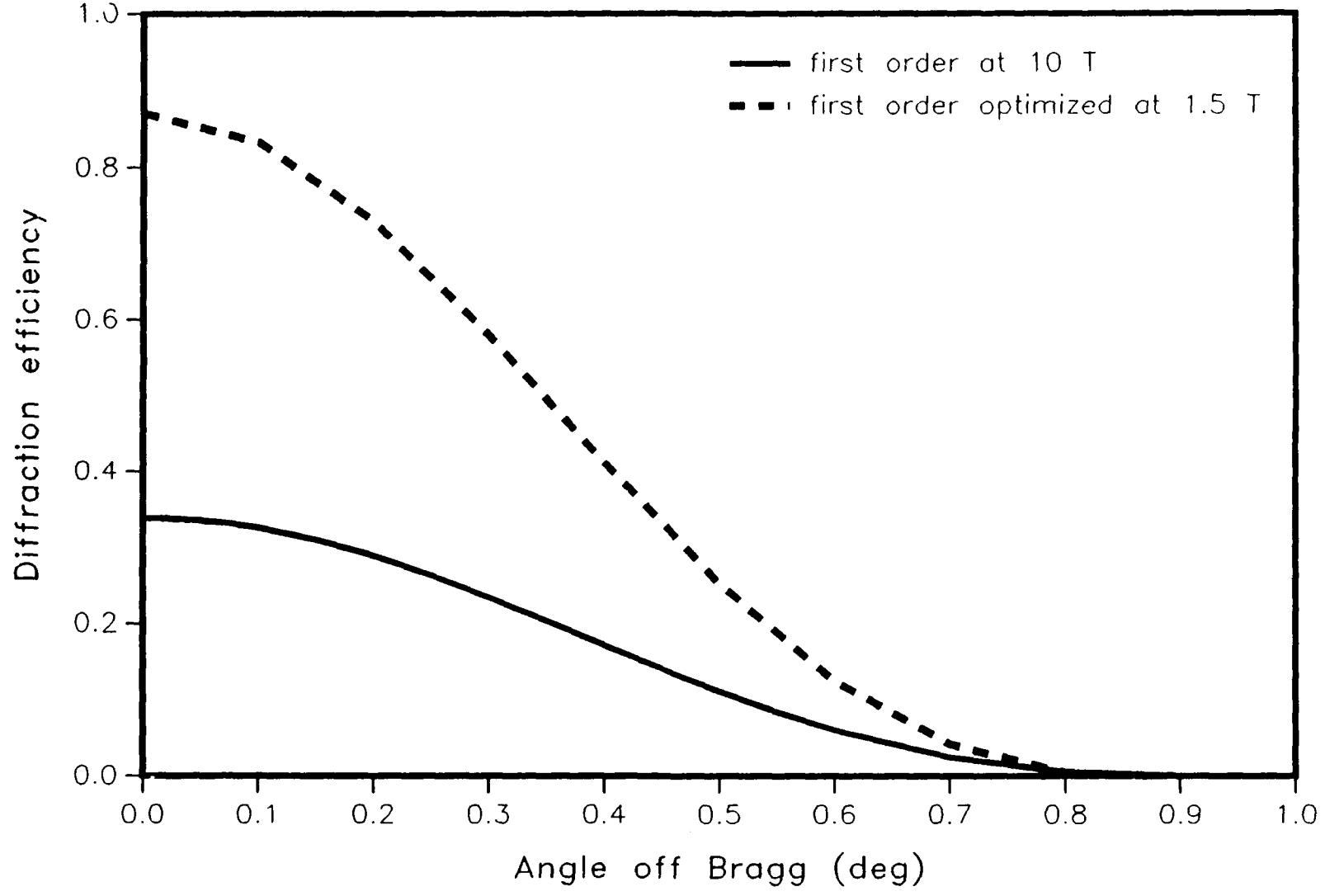

Figure 2.1.5 Sensitivity of first order diffraction efficiency to departures from Bragg angle: grating thickness, 1 mm

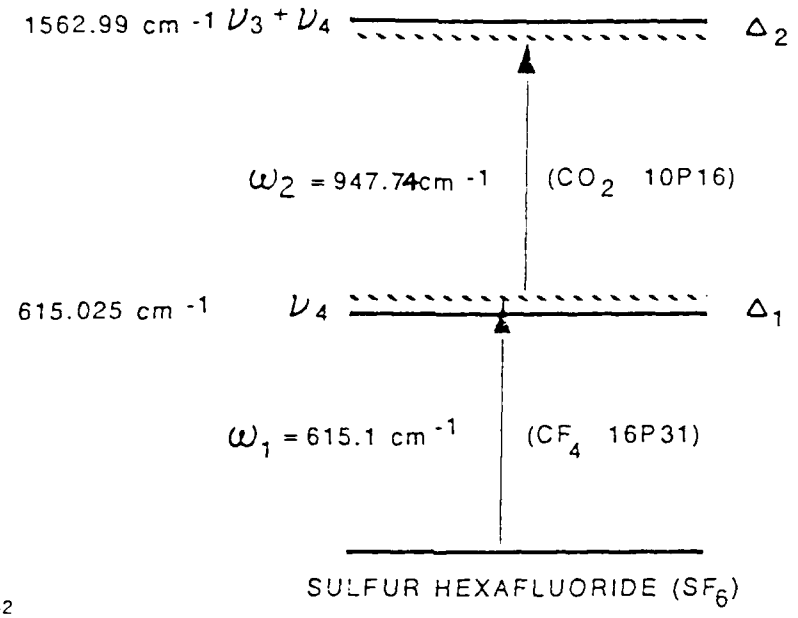

Figure 2.1.6 Level diagram for near-resonance nonlinear dispersion in SF_6. The energy given for $\nu 4$ is the Q-branch absorption edge. $\nu 3$ is taken as 947.97 cm^{-1}. Thus $\Delta_1=(\omega_1-\nu_4) \approx$ 0.08 cm^{-1} and $\Delta_2=(\nu_3+\nu_4)-(\omega_1+\omega_2)\approx 0.15$ cm^{-1}.

We next chose to examine grating shape as a function of pump and probe strength at different gas sample pressures. It is interesting to reconstruct how this came about. The original work on grating shape was done using the low field strengths appropriate for our early experimental setup. Thus in the early modeling runs, an elementary grating profile showed a $\sin^2$ shape. Doubling the pump field strength had the effect of leveling off the top of the grating profile, verifying that our approach could correctly model saturation effects, in contrast to the perturbative technique used by Rokni-Flusberg.[2] But we had recently noticed in the work on the effect of detuning that grating shape changed dramatically as the test pump frequency was brought closer to the absorption edge of the SF_6; the $\sin^2$ shape was characteristic of low pump and probe intensities and large detunings. As the pump frequency approached the absorption edge, the change in the real part of the index increased, but the center part of the grating profile flattened out and even became depressed. Furthermore, with the experimental improvements, we had larger field strengths available than previously, and saturation effects would likely be more pronounced.

The first step was to re-examine grating shape around the pump = probe = 1 sV/cm condition originally used at 0.1 Torr pressure with the best values of laser frequencies and SF_6 energy levels available. Results are shown in Figure 2.1.7. Here one finds that the probe field strength affects grating shape (as seen by the probe) as well as the pump field strength. The combination (not shown) of pump at 1 sV/cm, probe at 0.1 sV/cm, produces a nice $\sin^2$ shape.

Figure 2.1.8 shows the calculated grating shapes for SF_6 pressure at 10 Torr, other conditions the same. It is immediately apparent that the shapes are almost identical while the magnitudes scale by the pressure ratio. It is interesting that in any of the cases shown, for probe incidence at the Bragg angle, virtually all of the diffracted energy goes into the zero order or first order diffraction (depending on grating thickness) or is absorbed. We note again that the basic grating periodicity is set by the angle between the two pump beams (60°) and the pump wavelength (16.26 μm); the possible number of propagating diffracted orders are then determined from the Bragg condition, which involves the probe wavelength in the medium. Thus the only other orders allowed are -1 and +2, and virtually no power goes into these.

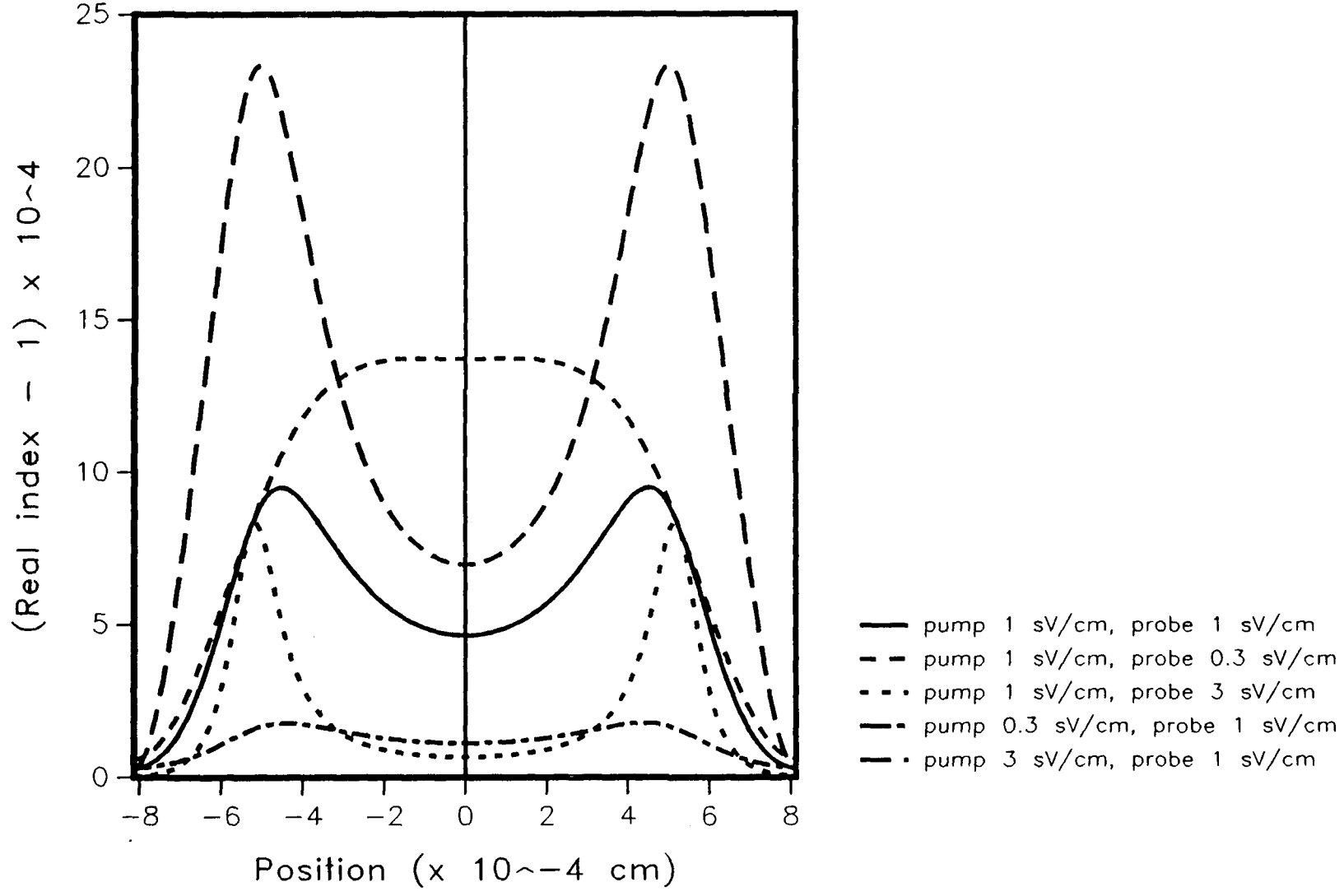

Figure 2.1.7 Effect of field strength on grating profile; SF_6 pressure, 0.1 Torr

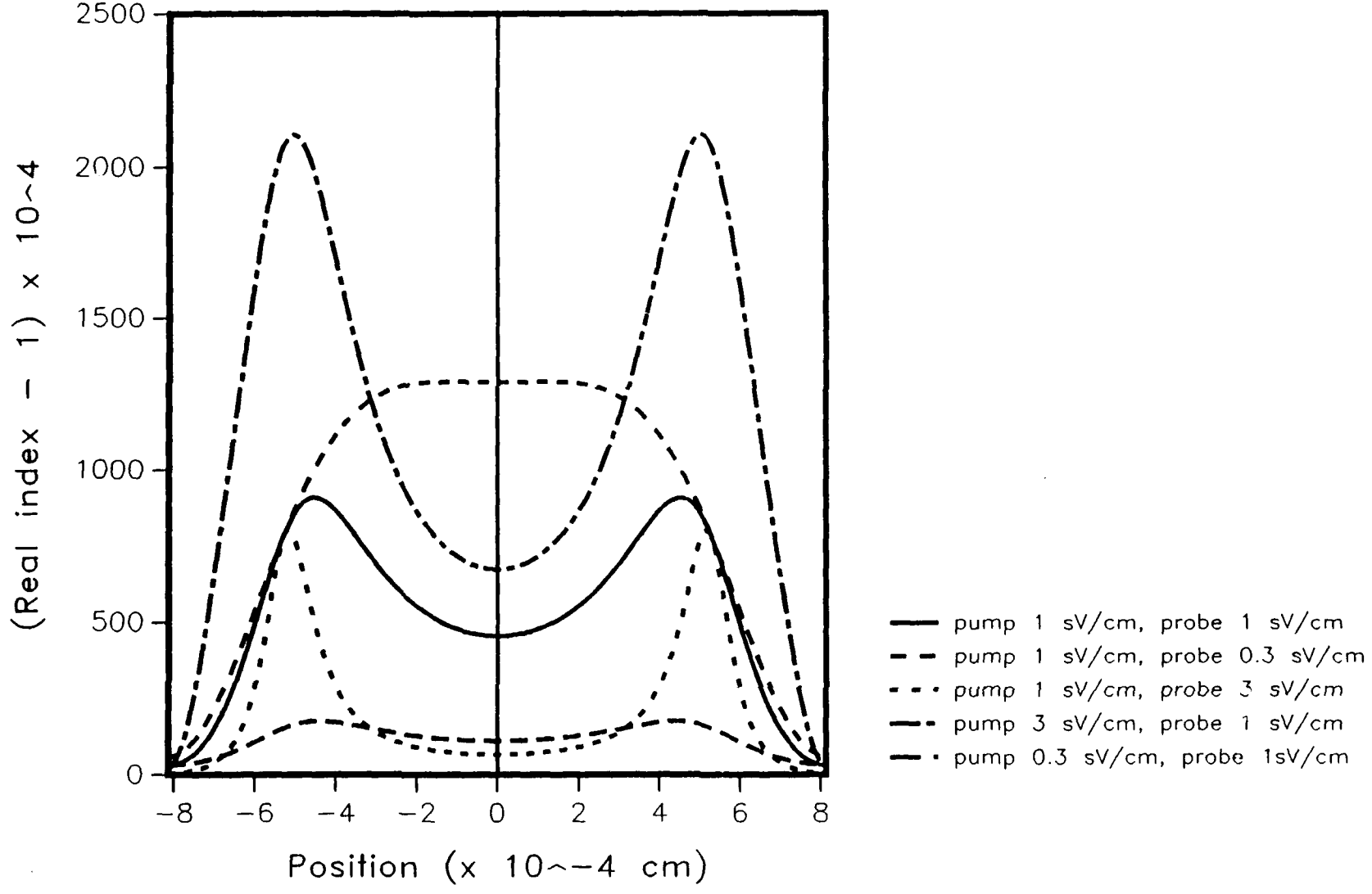

Figure 2.1.8 Effect of field strength on grating profile;
SF_6 pressure 10 Torr

At this point in time, data acquired with the improved experimental setup showed that we had substantially more pump power available than originally, and we anticipated an easier job of demonstrating a grating. Data showed that we could expect maximum pump field strength near 5 sV/cm. Figure 2.1.9 shows zero and first order diffraction efficiency vs position through the grating at 10 Torr for equal pump and probe field strengths of 4.85 sV/cm. Note that for D = 1 mm, $D/\Lambda = 61.5$. The behavior shown in Figure 2.1.9 is exactly what is expected for a strong phase grating with some absorption.[7] However, at a given grating thickness, changes in the magnitude of the index change (Δn) also can make the diffraction efficiencies oscillate, exchanging energies between zero and first orders, and making the experiment difficult to perform. Therefore we sought to optimize experimental conditions.

An obvious way to reduce the diffraction efficiency fluctuations at the given grating thickness while keeping the high field strengths was to reduce the SF_6 pressure. Figure 2.1.10 shows the effect of pressure on first order diffraction efficiency. Apparently near 1 Torr pressure is a good region to work, since first order diffraction efficiency is a reasonably sized fraction, and variations expected in field strengths during the course of the experiment, although affecting the magnitude, will not throw all of the power over into the zero order. Thus settling near 1 Torr, grating shapes and first order diffraction efficiencies are shown in Figures 2.1.11 and 2.1.12 respectively for various probe field strengths.

As a final iteration to optimize the experimental conditions, a maximum indicated first order diffraction efficiency was sought for pump = probe = 4.85 sV/cm for the 1 mm cell thickness. At 1.5 Torr, first order diffraction efficiency was calculated to be 87%, with zero order near 7%•(the rest is absorbed). Under these conditions, fluctuations in the field strengths will have minor effect on the diffraction efficiencies because of operating near a broad maximum.

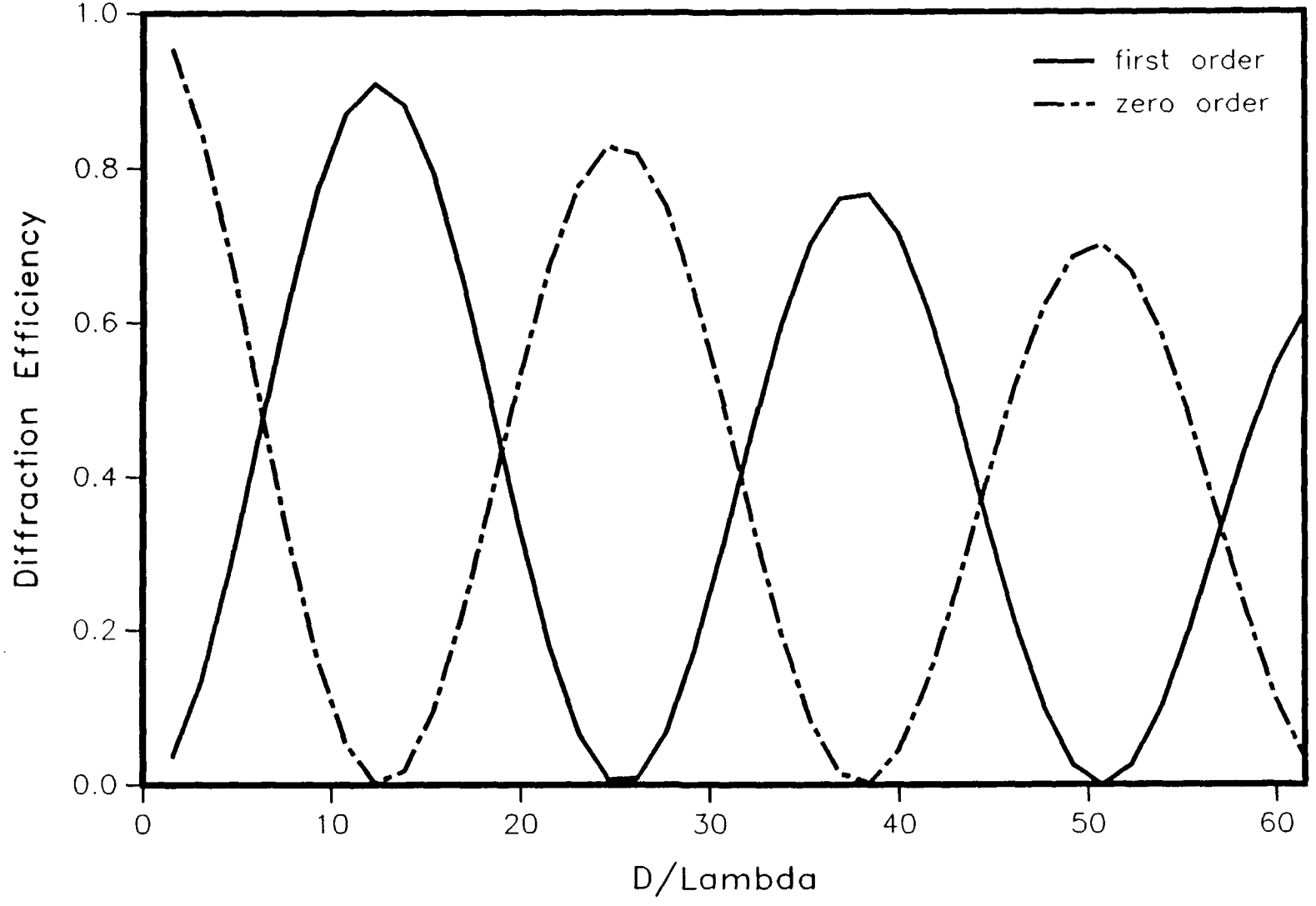

Figure 2.1.9 Diffraction efficiency at 10 Torr; pump and probe field strengths are both 4.85 kV/cm

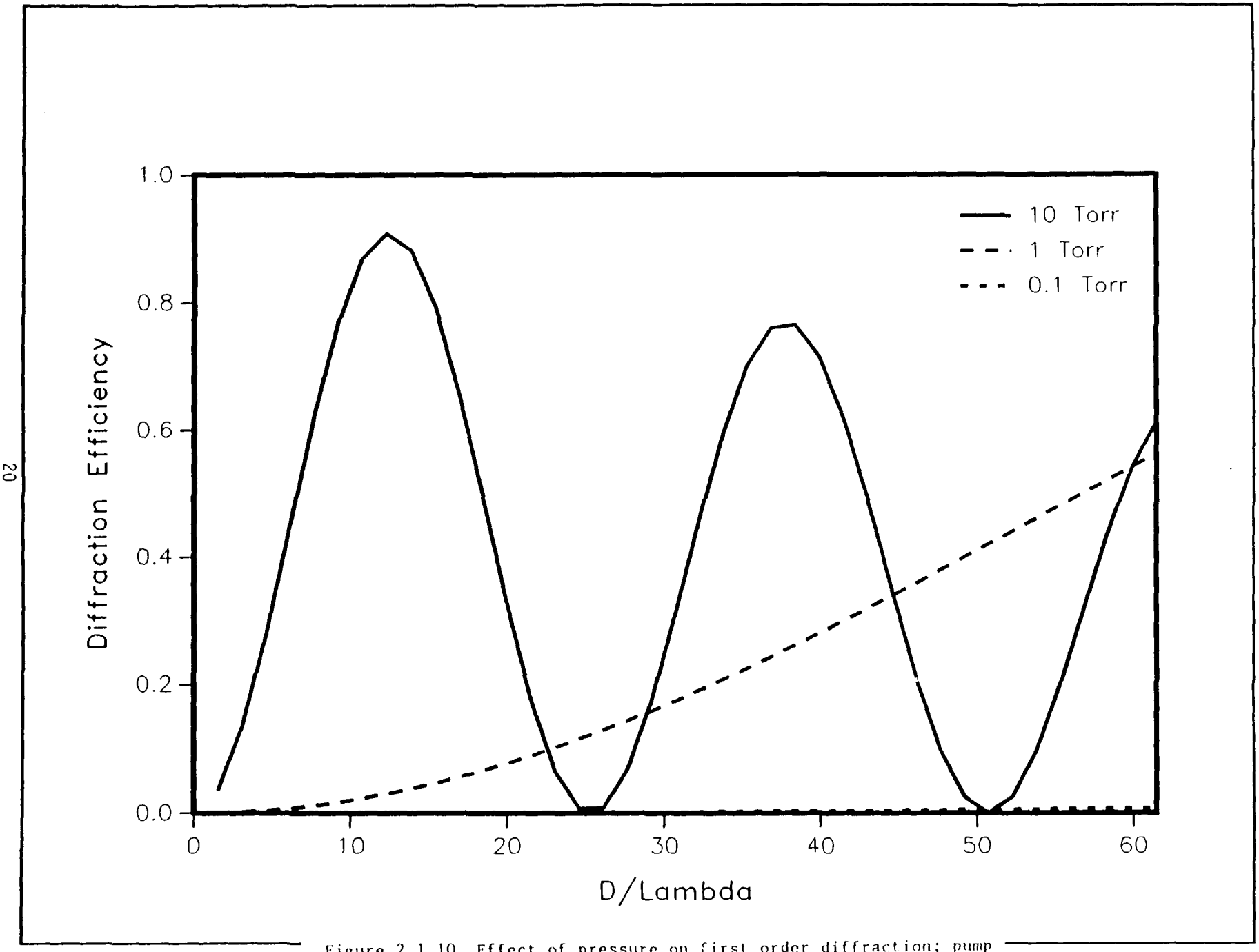

Figure 2.1.10 Effect of pressure on first order diffraction; pump and probe field strengths are both 4.85 sV/cm

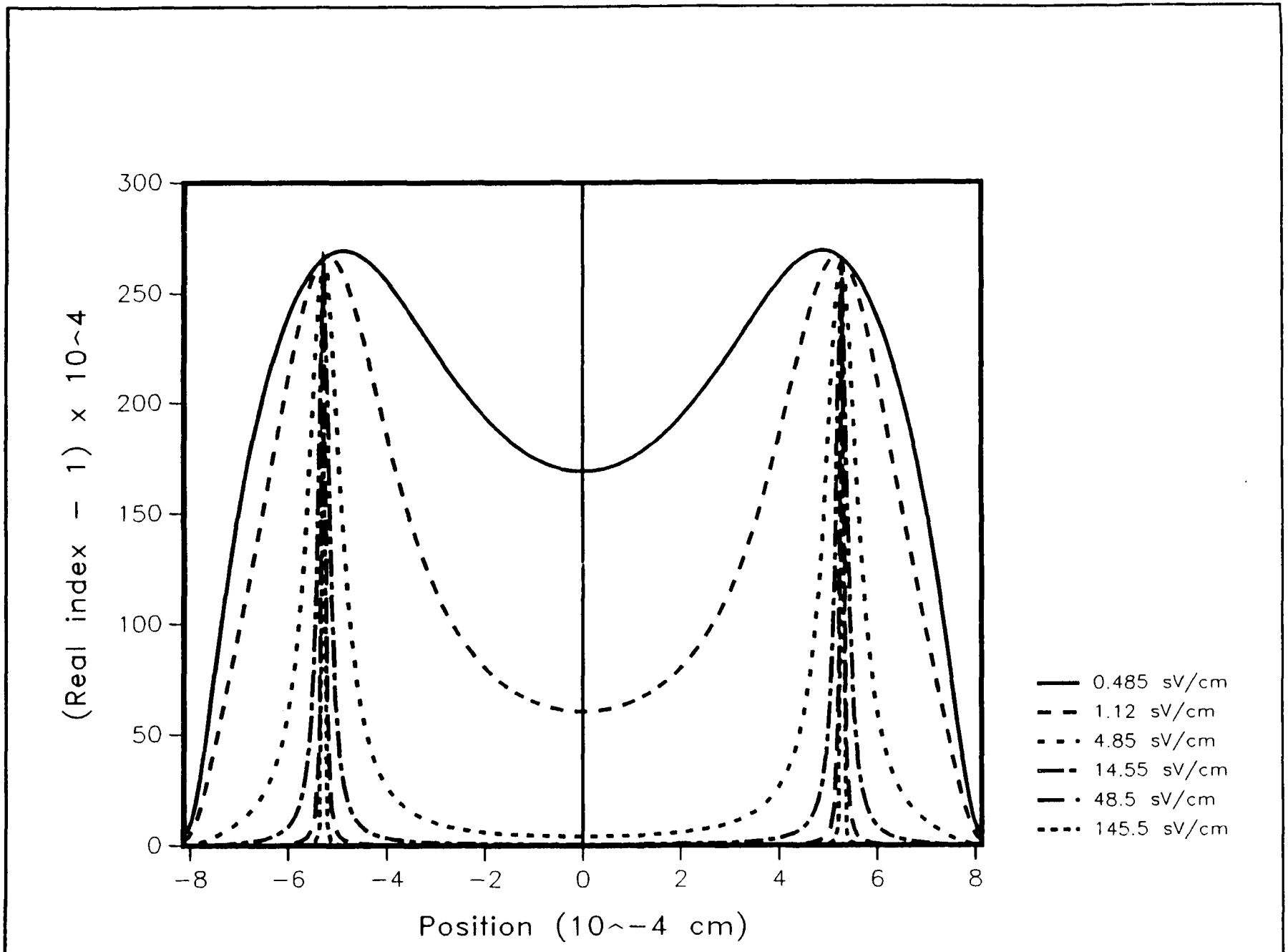

Figure 2.1.11 Effect of probe field strength on grating profile; pump field strength is 4.85 sV/cm; SF_6 pressure, 1 Torr

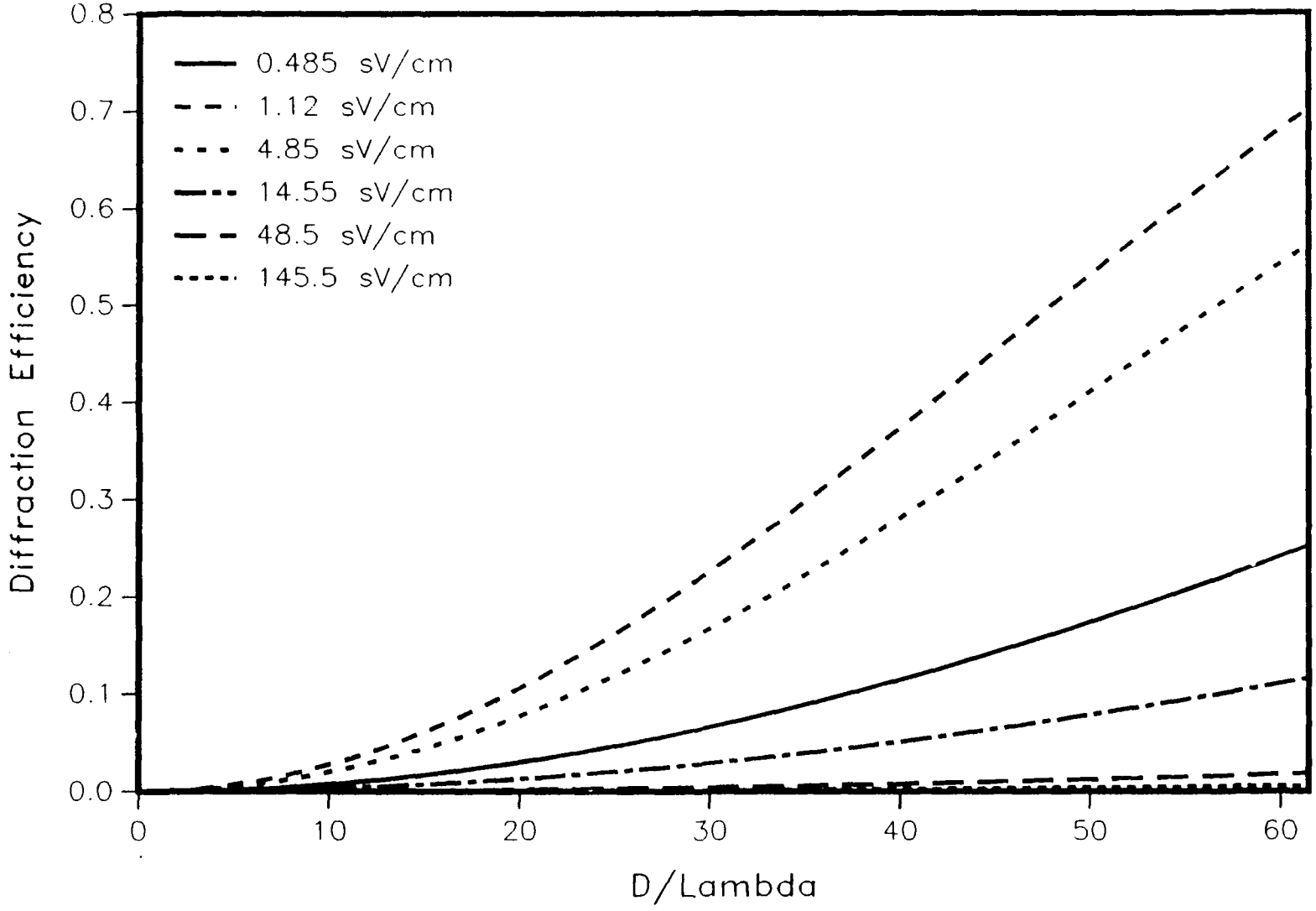

Figure 2.1.12 Diffraction efficiency at 1 Torr; pump field strength is 4.85 sV/cm; SF_6 pressure, 1 Torr

2.2 Task 2 - Experimental Media Investigations

2.2.1 Improvements to the Experimental Setup

A table layout for the experimental setup, roughly to scale, is shown in Figure 2.2.1.

As was pointed out in the report on the first year's work,[4] the CO_2 TEA laser (Laser 1, which pumped the CF_4 laser) was mounted separately from its low pressure gain cell on the optical bench. Each CO_2 gain section was originally supported on adjustable height lab jacks which were convenient for aligning the tubes' axes. We sought to relieve concerns about mechanical instability and long term height relaxation by removing the lab jacks and substituting large, precisely machined aluminum blocks for laser support. This substitution proved quite satisfactory; the only long term drift observed was thermal, and that was easily corrected by the piezo-drive on which the TEA laser output mirror was mounted.

One new CdTe Brewster window was obtained and installed on the CF_4 gain cell to replace the original window which had developed a crack and small leak. A 90% reflecting beam splitter was made on ZnSe in the LTV shops for sampling the 16.26 μm pump beam.

During the first year of this research, energy meters were used to detect 16.26 μm signals. Subsequently, two high speed photoconductive Ge:Cu detectors were installed into the apparatus (D_2 and D_5). The detector dewars had bottom (downward facing) windows, so the dewars were mounted above the integrating spheres used with them. These detectors operated at 4.2K, had responsivity near 0.11 A/W, and had D* (21 μm, 1000 Hz) $\geq 1.6 \times 10^9$ cm(Hz)$^{1/2}$/W. The detectors were followed by a video amplifier circuit, shown in Figure 2.2.2. The Comlinear Corp. video amplifiers (bandwidth $\geq$ 500 MHz, gain $\geq$ 10 dB) were mounted with their + and - 12V batteries in metal enclosures to defeat electromagnetic interference associated with the TEA lasers. The 80V bias necessary for the photoconductor detectors was provided by a separate power supply. With the Ge:Cu detectors, spatial and temporal diagnostics could be performed on the 16.26 μm pump beam from the CF_4 laser.

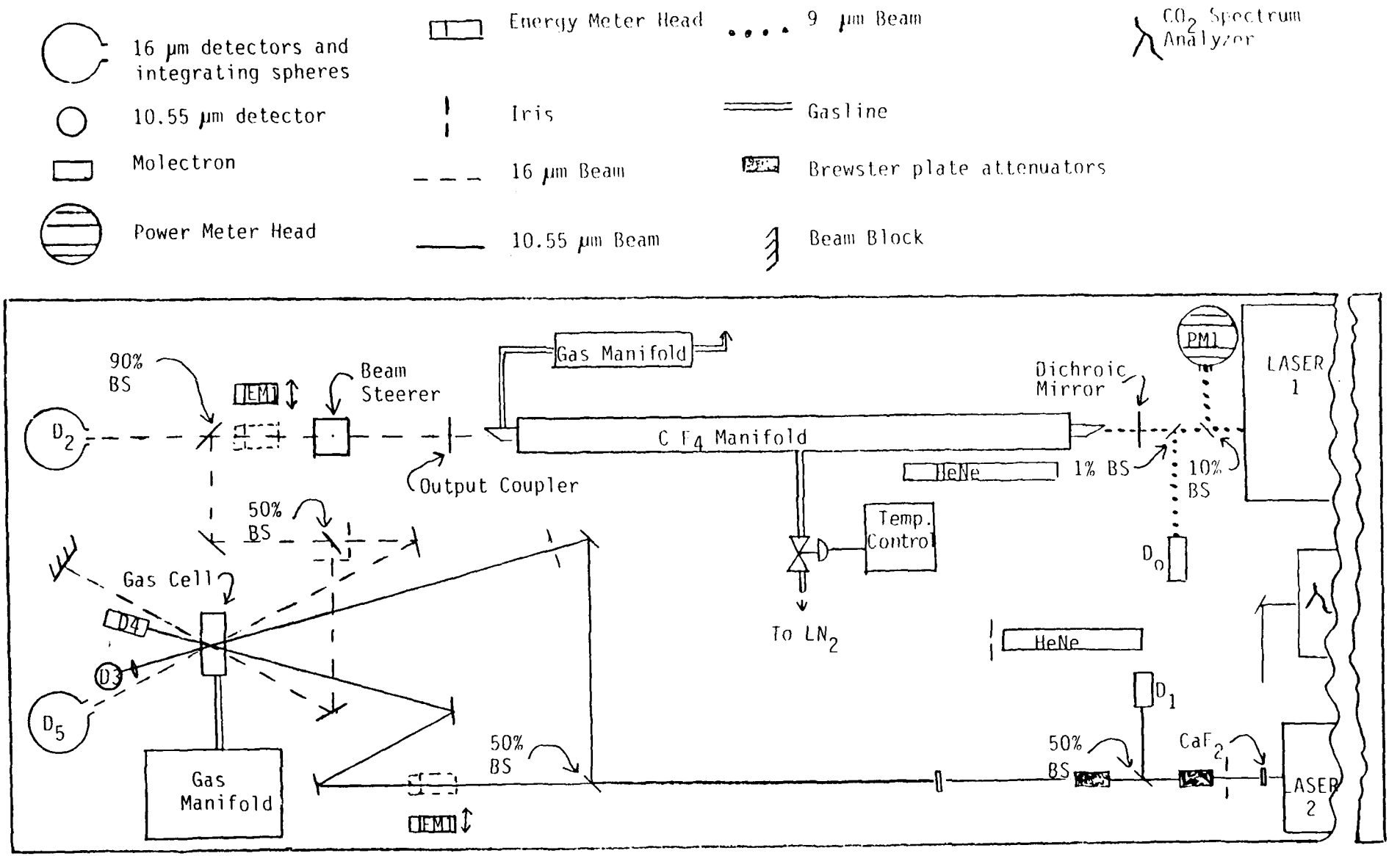

Figure 2.2.1 Experimental layout

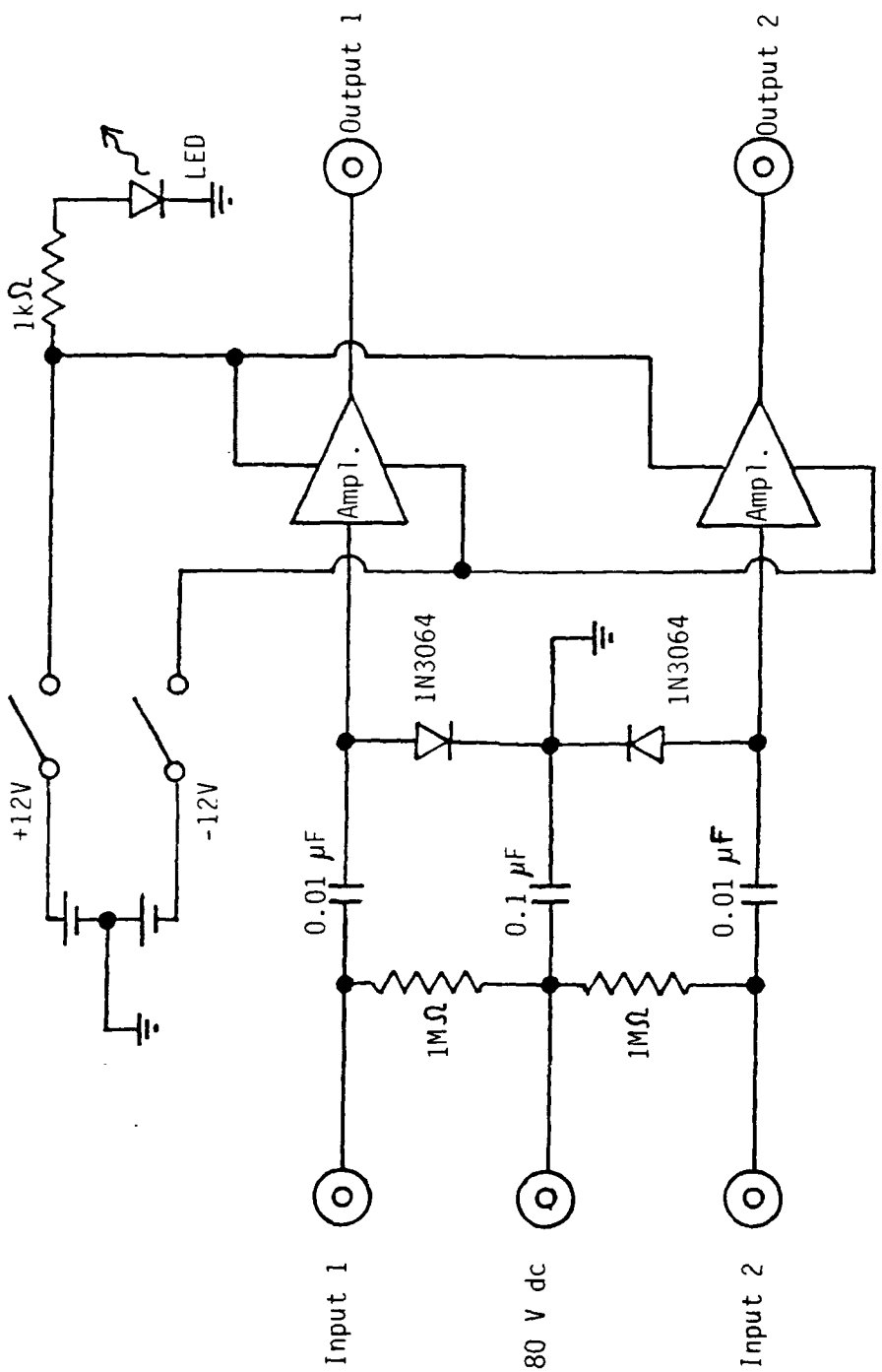

Figure 2.2.2 CLC100 video amplifier circuit

The pulse-pumped CO_2 laser which had been used as the probe laser was replaced by a small (mirror separation of 32 cm) CO_2 TEA laser (Laser 2 in Figure 2.2.1). A 150 line/mm grating was installed on an adjustable rotating mount as the back mirror of the replacement laser to provide for line selection. The LTV optics shop and thin film facility fabricated two flat ZnSe windows, each antireflection coated at 10.55 μm on both sides, to replace the poor quality gain cell closure windows (these were not Brewster windows). An aperture was installed just inside the output coupler to restrict the output to TEM_{00}. Under those conditions, total output energy at 10.55 μm was about 15 mJ, and attenuators were used to reduce probe energy. Two new 50% beam splitters were made at LTV to sample and distribute the probe beam(s).

In the final configuration, a pyroelectric detector (D_4) with a germanium collecting lens was used to monitor the straight-through (or zero order) probe beam. D_4 was followed by a broadband preamplifier. To seek diffracted probe energy, a photovoltaic HgCdTe detector (D_3) preceded by a collecting lens and followed by a fast preamplifier (also packaged against EMI) was used.

The use of the small CO_2 TEA laser as the probe laser improved the reliability of the pump/probe timing considerably. As shown in Figure 2.2.3, a function generator initiated the firing of the CO_2 TEA laser pumping the CF_4 laser. The timing of the probe laser pulse was controlled by the delayed signal from a pulse generator. Detector D_0, receiving a small fraction of energy from laser 1, provided the external trigger for the data recording apparatus.

A new sample cell was fabricated in which the window separation was 1 mm, thereby setting the grating thickness at 1 mm. Because the grating was to be created by two overlapping pump beams whose gaussian $1/e^2$ diameters were about 1 cm, the grating would be much more uniform across its thickness, as compared to the previous case in which the windows were separated by 1.57 cm. Again KBr windows were used on the cell. A new window had to be ordered to replace one which had developed a compression crack. The windows were retained by plates machined to hold two O-rings. One O-ring seals to the window, the other to the body of the mount, thus isolating the gas space. A diagram is shown in Figure 2.2.4.

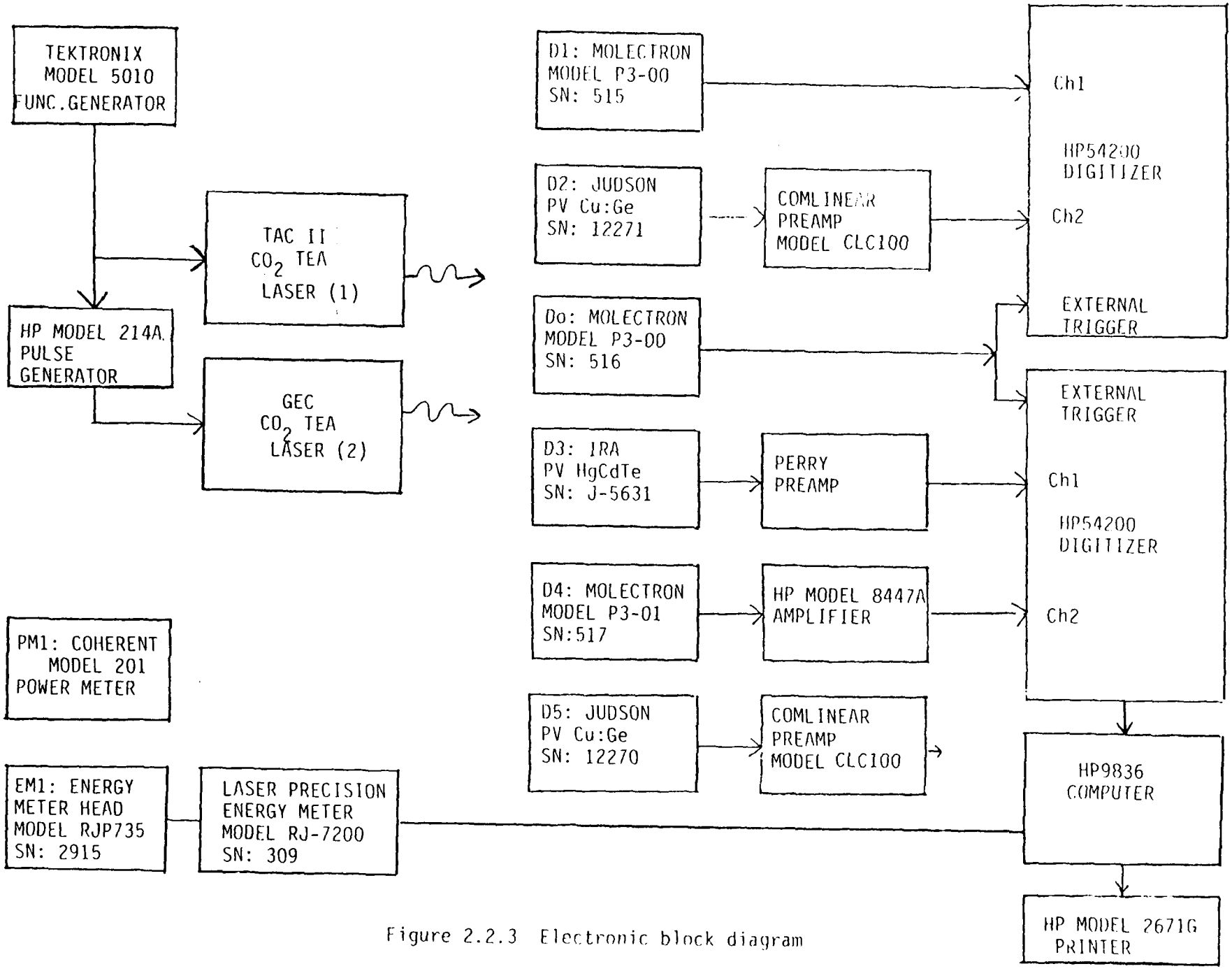

Figure 2.2.3 Electronic block diagram

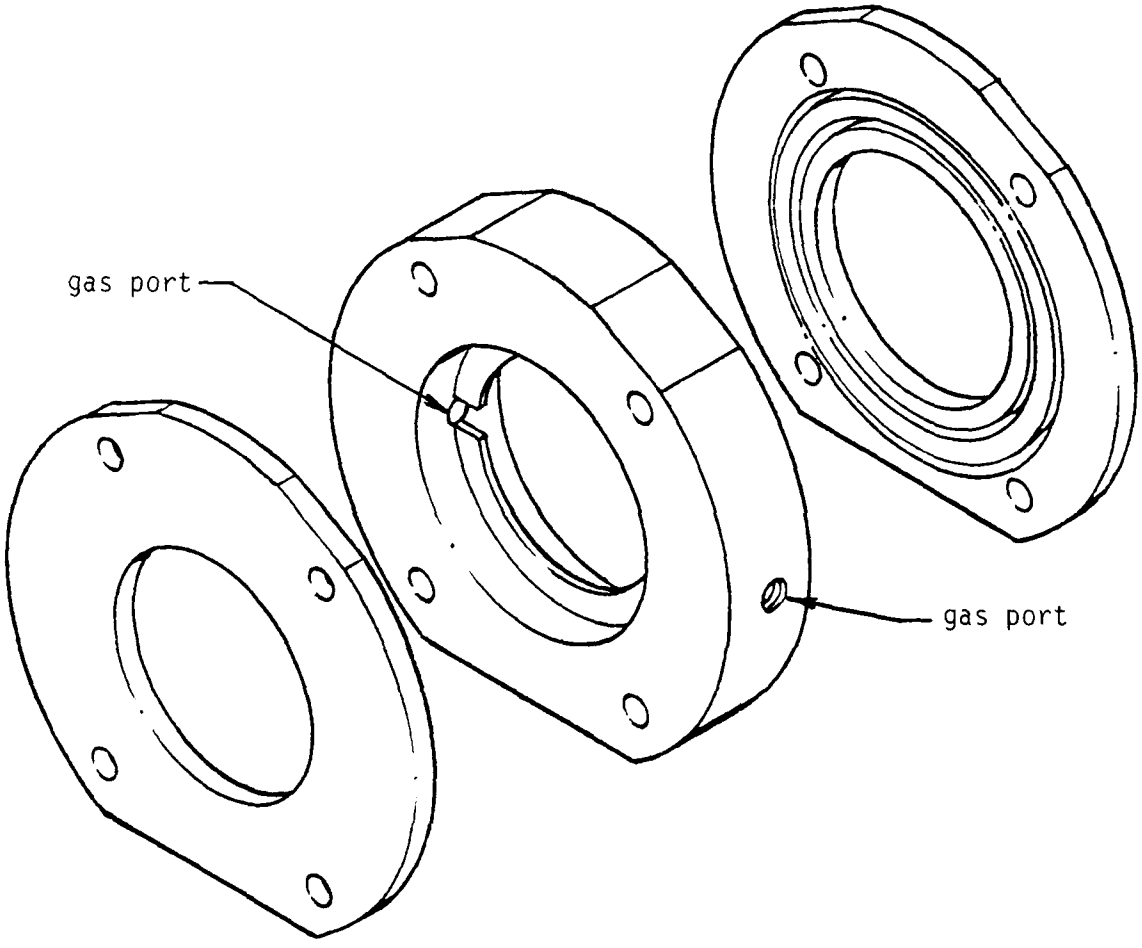

Figure 2.2.4 Sample cell assembly without windows

A new, tighter gas manifold was constructed for more precise control of SF_6 and buffer gas (if any) in the sample test cell. A thermocouple gauge was added for reading pressures less than 1 Torr, if used.

Figures 2.2.5, 2.2.6, and 2.2.7 are photographs of the apparatus from different angles. Figure 2.2.5 provides the best overall view. In it the small CO_2 TEA laser probe can be seen, with the pulse-pumped CO_2 laser (not in use) behind it. The sample cell and related gas manifold can be seen in Figure 2.2.6. The shielded battery supply and preamplifier cases for the Ge:Cu detectors are in the foreground on Figure 2.2.7. The liquid He dewars housing the Ge:Cu detectors, mounted above integrating spheres, are prominent in each photograph. The sample cell, visible in each picture, probably shows up best in Figure 2.2.7.

2.2.2 Results

The spatial power distribution or beam profile of both the 16.26 μm pump beam and 10.55 μm probe beam is determined by stepping an appropriately sized pinhole across the beam in a number of steps. The power transmitted by the pinhole is measured at each step while simultaneously sampling the power of the full beam. The data processing software integrates pulse power vs time to give received energy per pulse, and then takes the ratio of the energy through the pinhole to the energy of the full spatial pulse for each step. A plot of the ratio at each step thus provides a map of beam's spatial power (or energy) distribution.

For the 16.26 μm pump, a 2 mm diameter pinhole with a Ge:Cu detector behind it was stepped across the beam in 1.5 mm steps. A measured beam profile is shown in Figure 2.2.8 superimposed on a gaussian profile drawn to the same $1/e^2$ power points. The measured $1/e^2$ beam diameter is 7.9 mm; the value at the measuring location, calculated from the laser mirror separation and curvature, is 10.2 mm. The calculated diameter is 30% larger than the measured value, although one notes that the measurement was made inside the Rayleigh range of the CF_4 laser, so that the calculated value at the measurement distance is not terribly reliable. The 16.26 μm beam diameter at the sample cell the distance to which is roughly equal to the laser Rayleigh range, is calculated to be 11.8 mm.

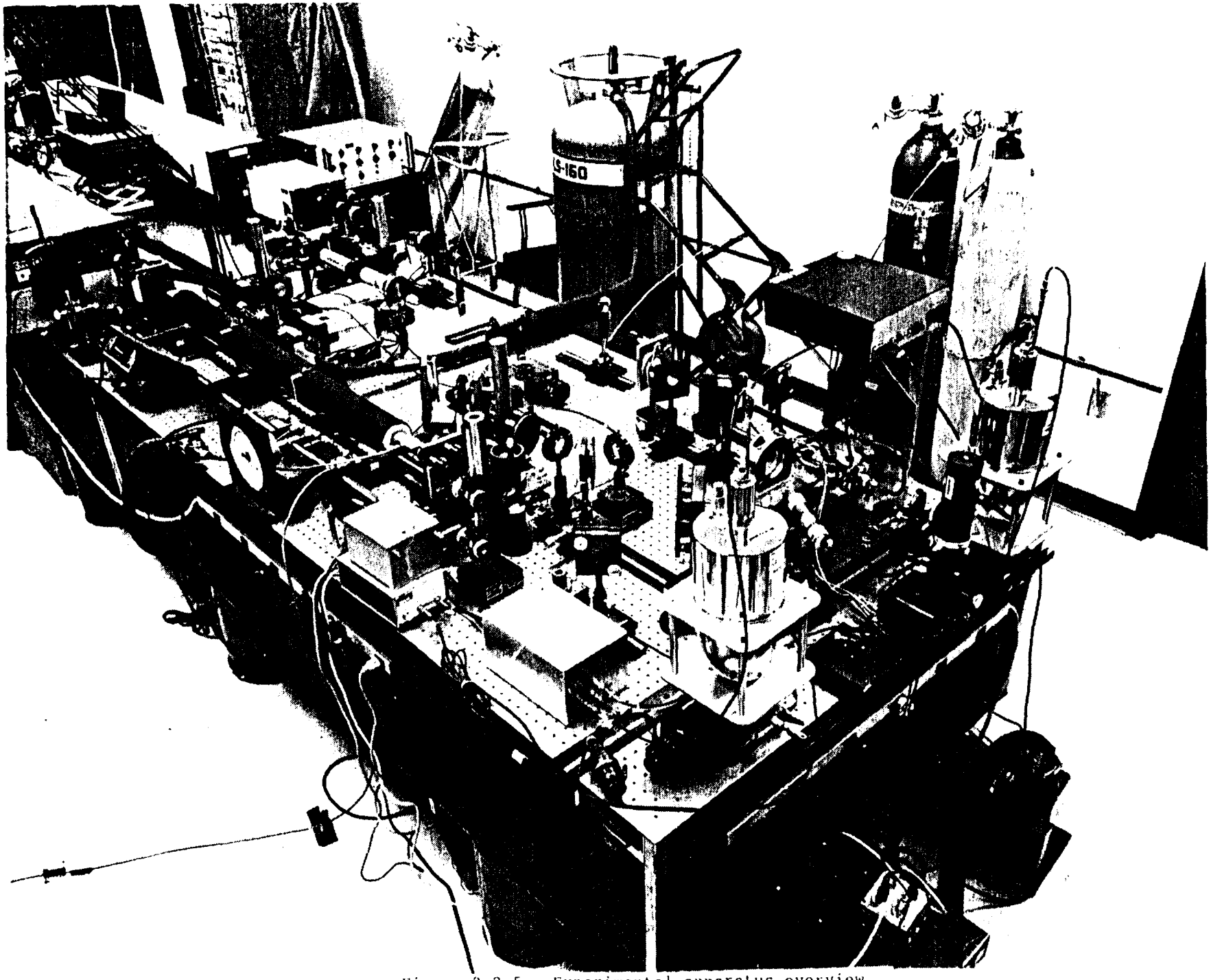

Figure 2.2.5 Experimental apparatus overview

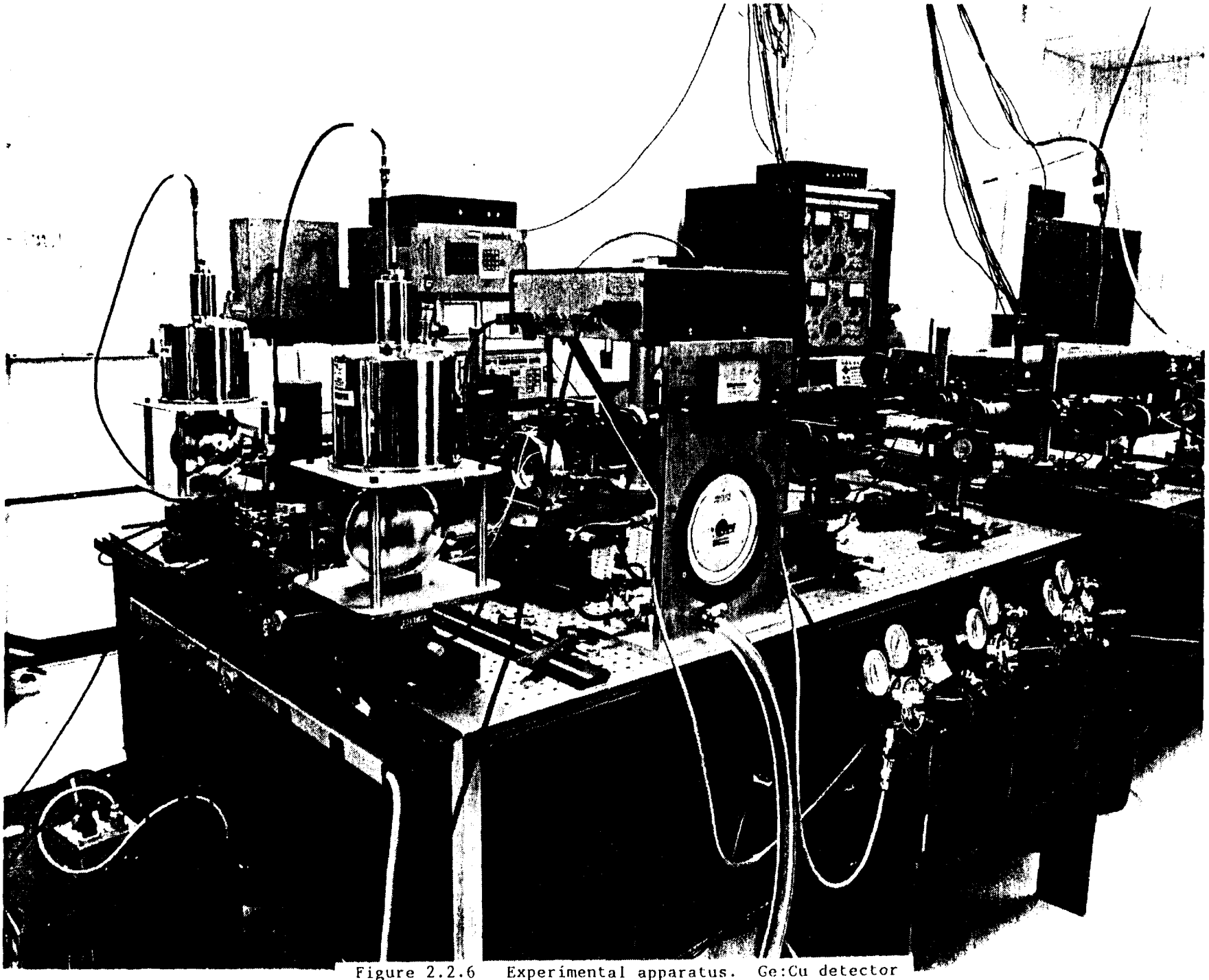

Figure 2.2.6 Experimental apparatus. Ge:Cu detector dewars and gas manifold in foreground.

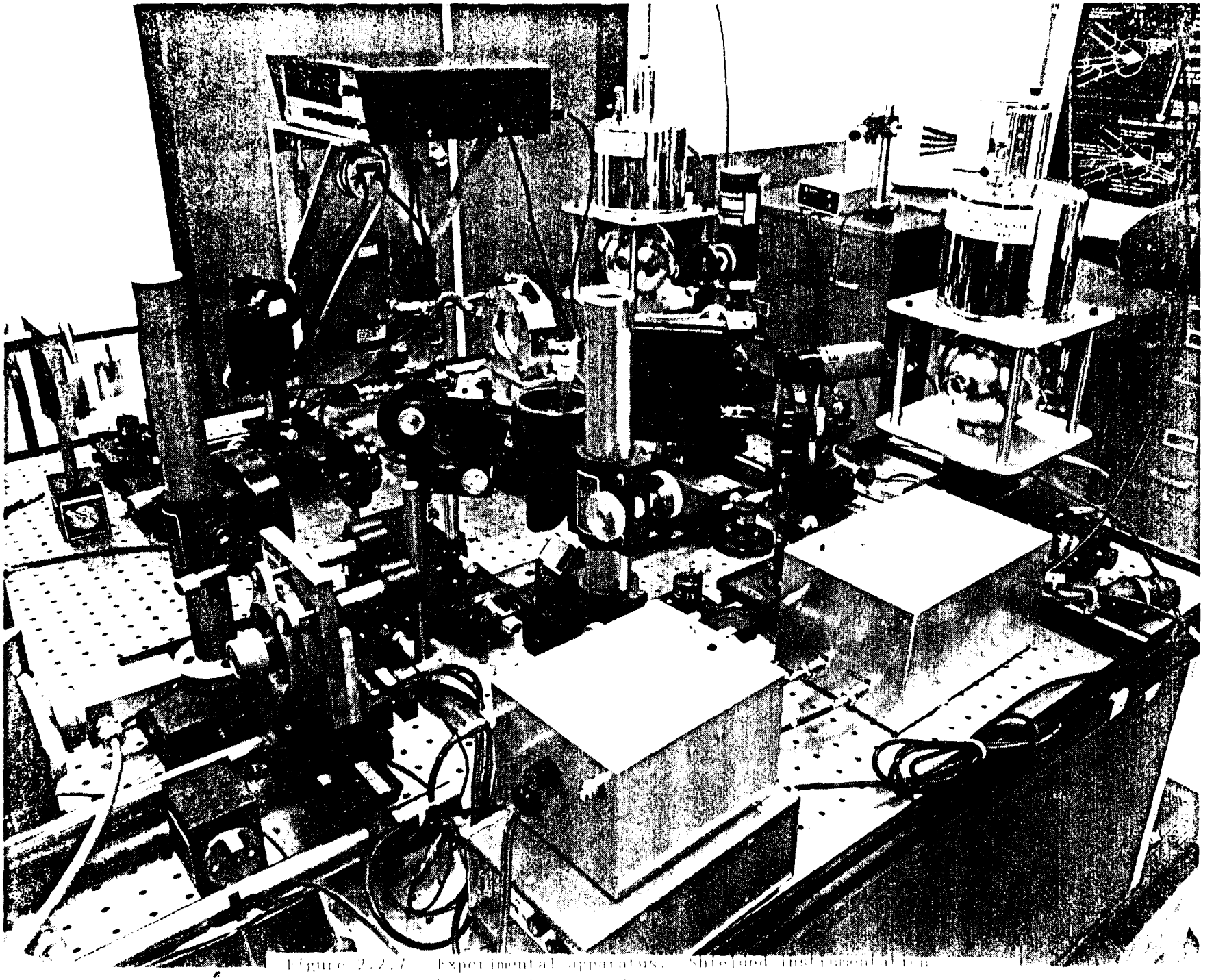

Figure 2.2.7 Experimental apparatus. Shielded instrumental tra

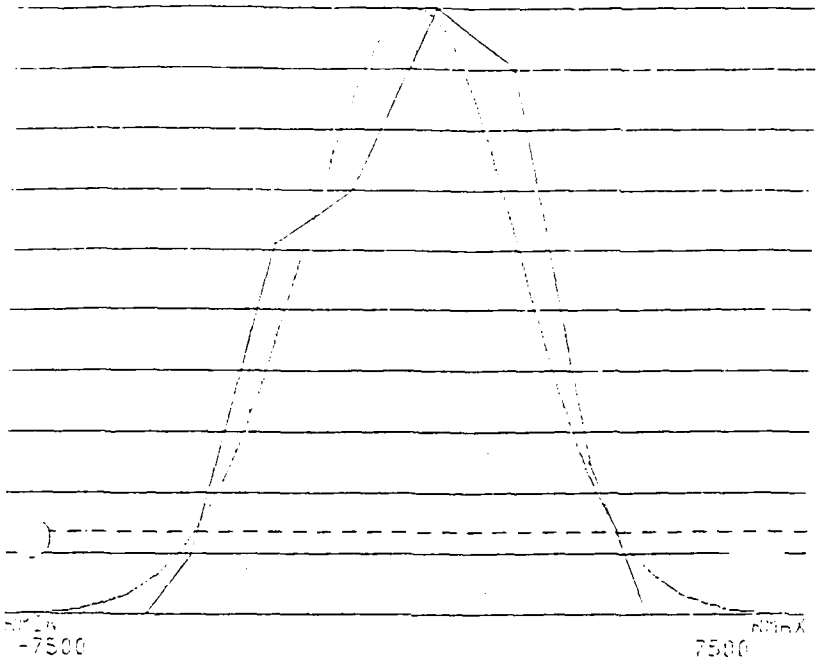

Figure 2.2.8 Spatial profile of 16.26 μm pump beam

Care was taken to assure that the pump beam paths after the 50% beam splitter in the 16.26 μm beam line (see Figure 2.2.1) were as equal as possible; measurements indicate that the path difference was less than 1 cm over average split paths of 75 cm.

With the 10.55 μm probe beam, a 1 mm pinhole in front of a pyroelectric detector was scanned across the beam in 1.05 mm steps. The measured beam profile superimposed on a gaussian of the same $1/e^2$ width is shown in Figure 2.2.9. Here the beam diameter was measured beyond the Rayleigh range; measured value was 7.5 mm compared to calculated 7.2 mm, roughly 4% difference. The $1/e^2$ diameter at the sample cell was calculated to be 10.6 mm.

The match between the diameters of the pump and probe beams at the cell, calculated to be 11.8 mm and 10.6 mm respectively, is seen to be satisfactory. However, it is also important that the angles of incidence be set at the correct values, even though the angular sensitivity with the 1 mm thick grating is much reduced compared to the previous 1.57 cm thick grating. The calculation of the angular sensitivity made in section 2.1 assumed a grating spacing of 16.26 μm created by the pump beams intersecting at exact 60°. Satisfying the Bragg condition of course depends on both the incident angle of the probe and the grating spacing. Angles in the experimental apparatus are set using a HeNe alignment laser and two irises to insure that the infrared beam (16.26 or 10.55 μm) traces the HeNe beam. The sample cell is mounted on a rotating base with vernier degree scale. The precision and repeatabilty of the rotating base, the errors in setting the irises, and the errors in aligning the IR beams with the irises all contribute to the experimental error. We find the expected experimental uncertainty in the Bragg angle to be $\pm 0.5°$. Considering the predicted angular sensitivity of $\pm 0.4°$ (FWHM), this experimental uncertainty is acceptable. Furthermore, a micrometer drive is provided on the final directing mirror of the probe beam, so that if any diffracted power at all is observed, the final mirror can be rotated horizontally to optimize Bragg angle setting.

With the fast detectors now available, the temporal profiles of the pump and probe lasers were measured. The full width at half maximum (FWHM) of the TEA-laser-driven 16.26 μm pump was characteristically 50-60 ns, and FWHM of the 10.55 μm probe pulse was somewhat wider, about 75-90 ns.

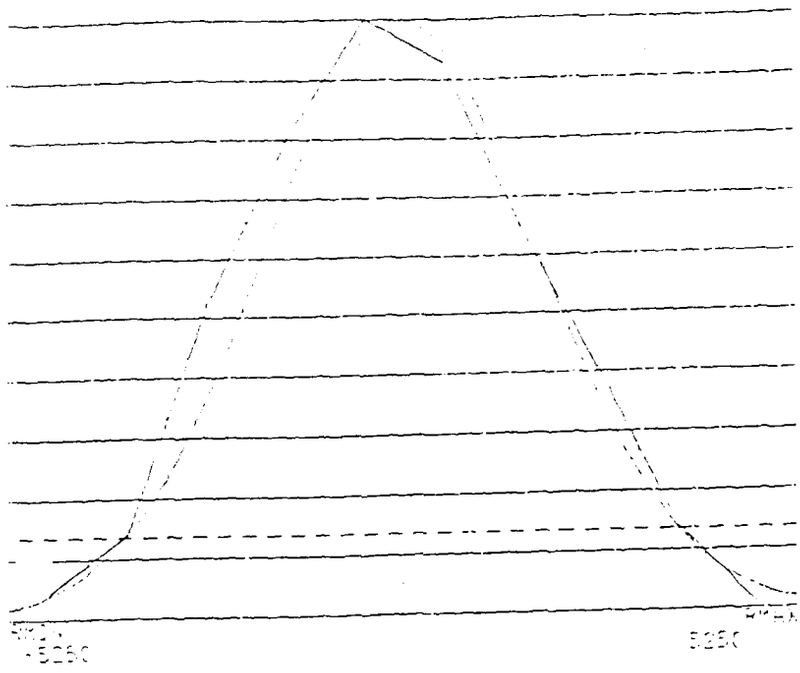

Figure 2.2.9 Spatial profile of 10.55 μm probe beam

The importance of having a known temporal relationship between the pump and probe pulses as well as a spatial overlap in the sample region cannot be overemphasized. Although a grating once established will have a finite decay time, this time may well be short. Factors which influence temporal uncertainty will include times of flight for the pulses, detector response times, delays in preamps, and cable transit times. Times of flight can of course be calculated. We note that the distance from the CF_4 output coupler to the sample cell was 184 cm; from the probe laser to the cell, 307 cm, a difference of 123 cm. At the speed of light, this accounts for 4 ns. We verified early that the three pyroelectric detectors, D_0, D_1, and D_4 had no relative delays. Addition of the preamp after D_4 added ~25 ns delay. The preamps following the GeCu detectors D_2 and D_5 introduced about 10 ns delay. No delay was observed for the preamp following HgCdTe detector D_3. After carefully accounting for times of flight, electronic delays, and lengths of cable, the residual timing uncertainty between pump and probe pulses at the sample cell was less than 20 ns, thus assuring temporal overlap of pulses in the test cell.

Calibration of detectors was accomplished by comparing (amplified) detector output integrated over time with the output of an energy meter. When the equivalent energy at the detector location is measured, the software provides the necessary scale factor so that the (amplified) detector output can be plotted appropriately scaled as power vs time.[8]

The maximum peak power obtainable per 16.26 μm pump pulse was found to be near 1.5 kW per pump beam. Peak pump beam intensity is calculated in W/cm^2 using the beam radius; 1.5 kW translates into 4.85 sV/cm, which is the maximum of the peak spatial and temporal values of the pump field strength, and the valued used in Figures 2.1.9 - 2.1.12. Typical peak power per pump beam was 1.2-1.4 kW, with energy per beam around 300 μJ.

With 15-20 mJ TEM_{oo} available from the probe TEA laser, its output was attenuated for use. Probe power density at the sample cell could easily be varied from a fraction of pump beam intensity to much larger than pump intensity. We typically operated from near 100 W to 1.5 kW peak probe power (probe energy ~20-300 μJ).

The first attempts to create and demonstrate a grating in this series of measurements were done at 10 Torr and 5 Torr pressure of pure SF_6. The peak pump power (per beam) at the sample cell was in the 1-1.25 kW range (~4-4.4 sV/cm); peak probe power at the cell ranged from 90-120 W (~1.25-1.45 sV/cm). The detector D_3 sensitivity and the ambient noise floor were such that diffracted power above 0.1 W or diffracted energy above 0.1 μJ could have been detected easily. That is, had diffraction efficiency for the probe beam into first order been as large as 0.1%, the apparatus would have detected it.

Data from four detectors were recorded for each pulse: from detector D_1, scaled to read the incident 10.55 μm probe power at the sample cell; from D_2, the 16.26 μm pump power per beam at the cell; from D_3, first order diffracted 10.55 μm power; and from D_4, transmitted or zero order power at 10.55 μm. At one pressure, a data set was taken with one pump beam blocked, a condition for which no grating could be produced, and a data set was taken with both pump beams present, for which there should be a grating. No diffracted energy was observed at either 10 Torr or 5 Torr. The relative timing between pump and probe was varied; again no diffraction was observed. There was one tantalizing data set at 5 Torr for which the ratio of transmitted to incident probe power decreased when a grating should have been present; however, there was no noticeable change in power at the diffracted detector, and it must be concluded that we had observed a data point with unusually wide scatter.

It was at this point in time that the work referred to near the end of section 2.1 was done on optimizing the experimental conditions, since the optimization could be done with firm measured data. As indicated, 1.5 Torr SF_6 was chosen. The probe power was also increased so that peak probe power was about the same as peak pump power per beam.

A series of measurements (12 in all) was made at 1.5 Torr SF_6 pressure. Peak pump power per beam was 1.1-1.8 kW. Peak probe power was 0.95-1.3 kW. No diffracted energy was observed; again, any diffracted power above 0.1% diffraction efficiency would have been detected. A representative data set is shown in Figure 2.2.10. Within the experimental data scatter ($\pm$10%), no difference was observed in the ratio of transmitted probe power (zero order) to incident probe power when a grating should be there (both pump beams present) or for a no-grating condition (one pump beam blocked).

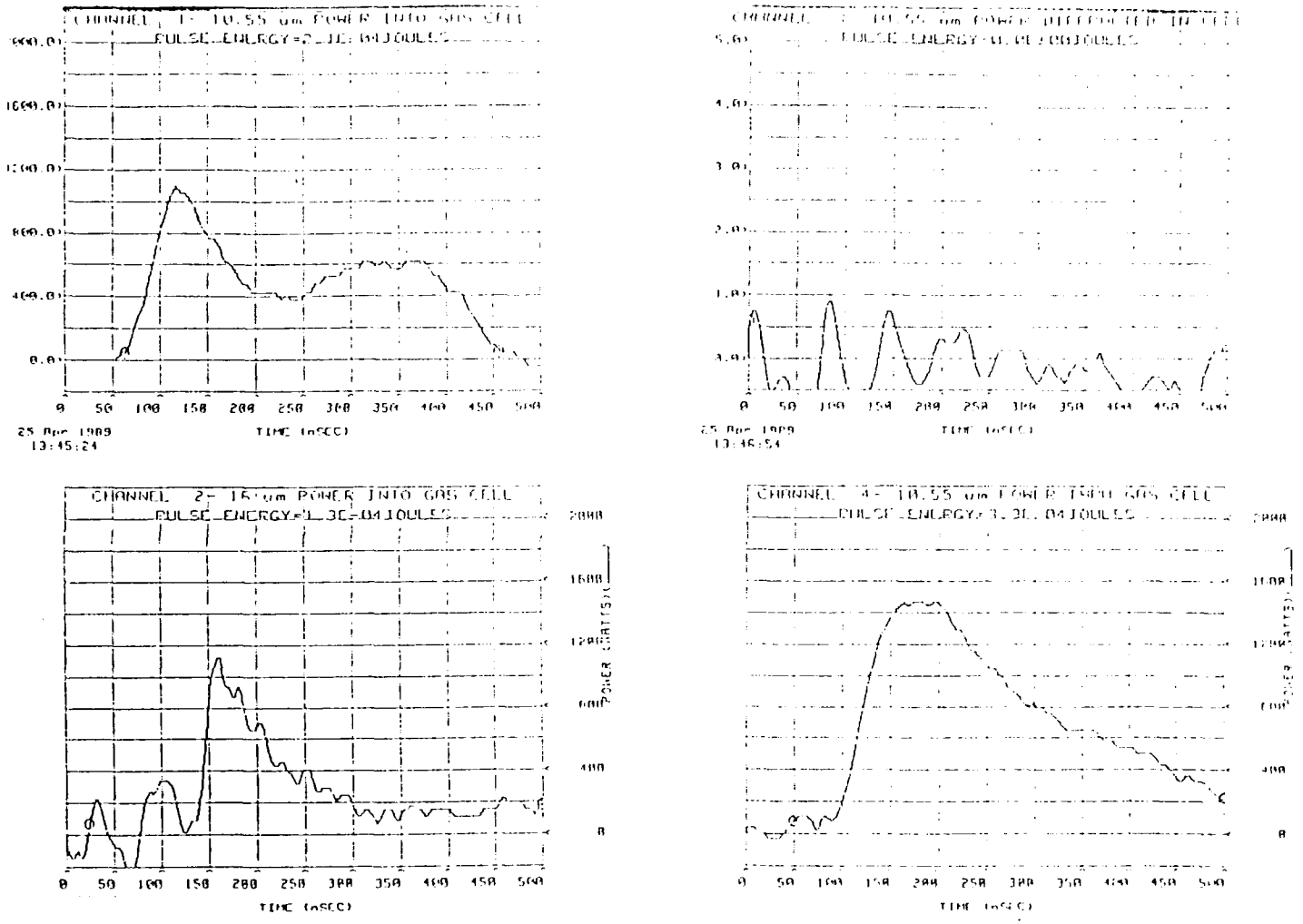

Figure 2.2.10 Typical data set while looking for diffracted energy

Experiments were run at 2 Torr and at 1 Torr with the same results: no diffraction observed. Evidence for a grating was then sought as the pressure was gradually reduced from 20 Torr to zero: again, no grating.

As a consequence of last year's discovery that the absorption of 16.26 μm radiation in SF_6 is affected by the presence of small amounts of helium, tests were conducted on the transmission of SF_6 to 16.26 μm in the presence of varying amounts of helium, argon, and xenon. Since the tests reported here were made using the 1 mm cell in place of the 1.57 cm cell, higher SF_6 pressure was needed to observe measureable amounts of absorption. Both Ge:Cu detectors were used, one to monitor the incident beam, the other, the transmitted beam.

The results of the 16.26 μm transmission experiments are shown in Figure 2.2.11. Although the data, which has been averaged and normalized, is somewhat scattered, there are some evident trends. At the higher SF_6 pressures (50 Torr and 25 Torr) used in these experiments, addition of helium does not have as pronounced an effect as at the lower pressure of 7.5 Torr used last year, but helium still appears to increase the transmission (decrease the absorption). Within the data scatter, both argon and xenon added into 25 Torr SF_6 suppress the transmission of 16.26 μm radiation, as opposed to the action of helium.

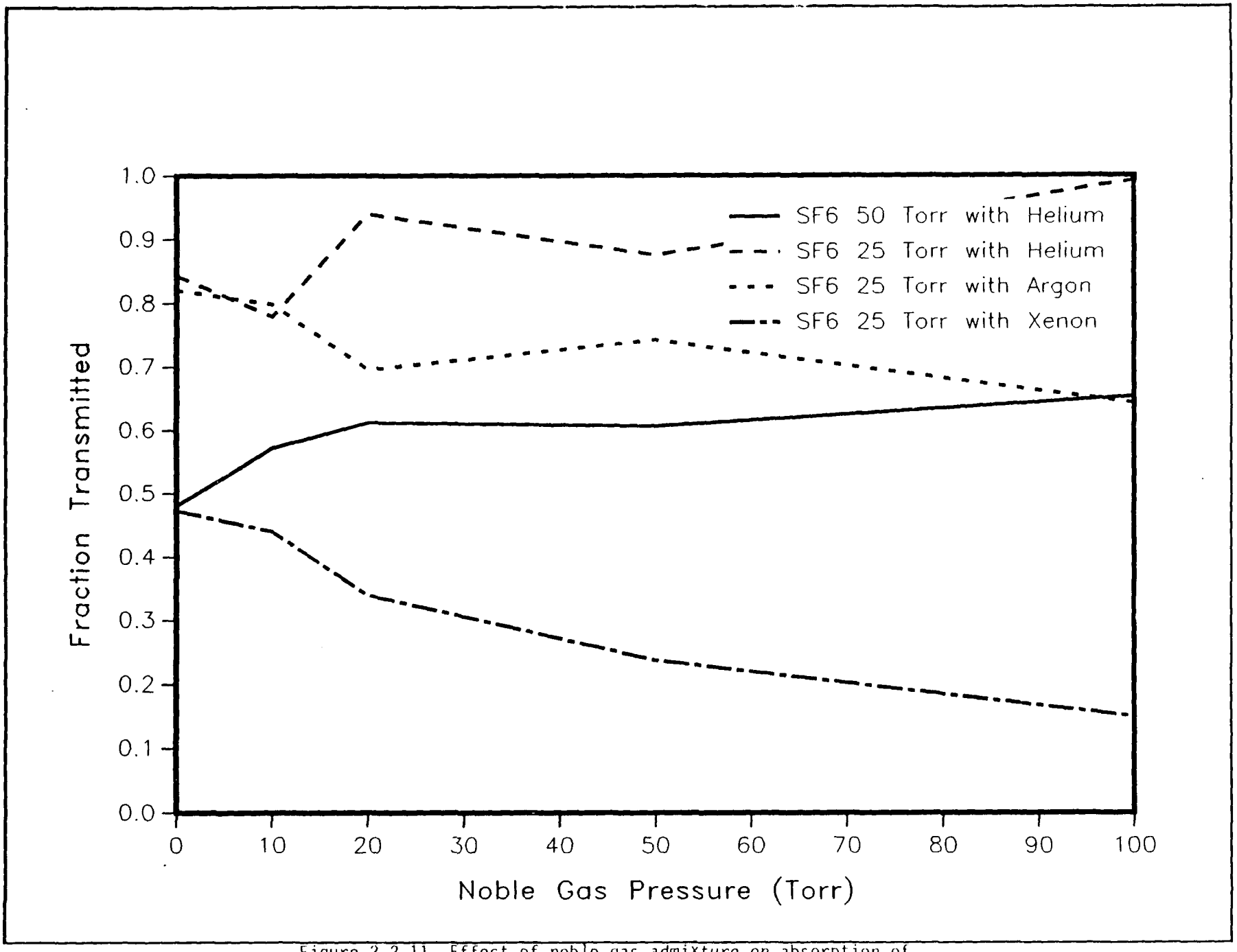

Figure 2.2.11 Effect of noble gas admixture on absorption of

3.0 CONCLUSIONS AND RECOMMENDATIONS

A nonperturbative analytical technique which allows for saturation effects was used to evaluate dispersion relations for a three level system for variable pump and probe frequencies and spatially varying field strength. The grating shapes thus generated formed the basis from which the probe beam interactions with the grating were determined using the coupled wave approach. The overall theoretical framework was used to predict viable experimental conditions based on expected parameters, to explore sensitivities to changes in experimental variables, and to suggest optimum values of controllable parameters when data began to be accumulated.

The experimental apparatus was modified to incorporate previously recommended improvements, a more satisfactory probe laser was installed, and new instrumentation was integrated into the setup. New data has been generated pointing to a shift of absorption energy levels in SF_6. The absorption of 16.26 μm radiation in SF_6 is seen to be unexpectedly sensitive to admixtures of noble gases.

However, despite the considerable interaction of theoretical and experimental effort, a laser-induced index-of-refraction, or phase, grating in a gaseous medium has not been demonstrated. Since the experiment was designed to detect very small amounts of diffracted energy and was relatively insensitive to changes in parameters, we must conclude that no grating was present.

It is unlikely that the predictions of Rokni-Flusberg[2] are entirely wrong since our analytical approach, which is less restrictive, gives similar predictions. Pressure-induced effects, although they broaden and sometimes cause shifts in spectral lines, do not appear likely to completely destroy an interaction in the case of pure SF_6. What may be more fundamental is that treating SF_6 as a simple three level system may be a gross oversimplification. Our model can be expanded to include more energy level structure in SF_6, but that would be a major undertaking.

It would be interesting to follow up on pressure-induced absorption changes in pure SF_6 and in SF_6 buffered with noble gases. Instruments exist which have

the necessary high resolution to quantify spectral shifts, although we do not have these available in our laboratories. We can easily investigate changes in absorption fraction of 16.26 μm at low SF_6 pressure and with various buffer gas mixtures by fabricating a longer path sample cell.

A further check can be made on our experimental apparatus by substituting for the SF_6 a medium in which we know a grating can be formed. A thin film of vanadium dioxide (VO_2) is such a medium. We note that phase conjugation by reflection from VO_2 has been observed at 10.6 μm,[9,10] and that the necessary optical properties extend to near 20 μm.[11] Research in this direction could easily be extended to evaluating the nonlinearity of VO_2, which has potential application to agile beam steering. Grating interaction in VO_2 can also be analyzed by coupled wave theory, although in this case the grating is a thin grating.

4.0 REFERENCES

1. "Coherent laser addition using binary phase gratings," J. R. Leger, G. J. Swanson, and W. B. Veldkamp, Appl. Opt. 26, 4391 (1987).

2. "Laser-Controlled Optics Using Near-Resonance Nonlinear Dispersion in Gaseous Media," M. Rokni and A. M. Flusberg, IEEE J. Quantum Electron, QE-20, 1324 (1984).

3. "Bragg Reflection by a Gain Medium Optically Pumped in a Grating Geometry," A. Flusberg and M. Rokni, IEEE J. Quantum Electron, QE-22, 730 (1986).

4. "A Nonlinear-Optical Method for Combining High Power Laser Beams in Gases or Plasmas," J. S. Chivian, C. D. Cantrell, III, C. A. Glosson, W. D. Cotten, S. F. DiMarco, and S. T. Garner, LTVMEG Report No. 3-45400/8R-66, 31 May 1988.

5. "Multilevel, Multifrequency Laser Pulse Propagation," D. R. Adams, C. D. Cantrell, and W. H. Louisell, Optics Comm. 43, 292 (1982).

6. "Analysis and Applications of Optical Diffraction by Gratings," T. K. Gaylord and M. G. Moharam, Proc. IEEE 73, 894 (1985).

7. See, for example, Laser-Induced Dynamic Gratings, by H. J. Eichler, P. Gunter, and D. W. Pohl, Springer-Verlag (1986); Section 4.3, Fig. 4.6.

8. A more detailed discussion of the calibration procedure can be found in "Computer-Controlled Facility for Laser Switching and Damage Testing," by J. S. Chivian, W. D. Cotten, D. F. Fuller, R. B. Hemphill, and M. W. Scott, in Laser Induced Damage in Optical Materials: 1985, NBS Special Publication 746, edited by H. E. Bennett, A. H. Geunther, D. Milam, and B. E. Newman, (U.S. Dept. of Commerce, 1988).

9. "Nonlinear interaction of infrared waves on a VO_2 surface at a semiconductor-metal phase transition," N. K. Berger, E. A. Zhukov, and V. V. Novokhatskii, Sov. J. Quantum Electron. 14, 505 (1984).

10. "Phase Conjugation via Reflection from VO_2," J. S. Chivian, Bull. Am. Phys. Soc. 32, 1179 (1987).

11. "Infrared optical properties of vanadium dioxide above and below the transition temperature, "A. S. Barker, Jr., H. W. Verleur, and H. J. Guggenheim, Phys. Rev. Lett. 17, 1286 (1966).

APPENDIX

Laser-Induced Gratings for Beam Manipulation in a Gas

by

Jay S. Chivian, W. D. Cotten, C. A. Glosson, and C. D. Cantrell

Presented at

OE/LASE '89
18 January 1989
Los Angeles, CA

Proc. SPIE 1060 (1989) (to be published)

Laser-Induced Gratings for Beam Manipulation in a Gas

Jay S. Chivian*, W. D. Cotten*, C. A. Glosson**, and C. D. Cantrell**

*LTV Missiles and Electronics Group, Missiles Division
P. O. Box 650003, Dallas, TX 75265

**University of Texas at Dallas, Center for Applied Optics
P. O. Box 830688, Richardson, TX 75083

ABSTRACT

Transient laser-induced gratings have been proposed as a means of controlling high power beams at a different frequency. Molecular absorption which shows an unusual sensitivity to buffer gas pressure has so far prevented observation of the desired grating.

1. INTRODUCTION

Near-resonance nonlinear dispersion has been suggested as a method by which a laser-induced grating may be created in a gaseous medium which has appropriate energy levels and transitions. In a collision-dominated gas, it is predicted that a strong field at one wavelength may be controlled by a weaker field at a different wavelength.[1,2] This then could form the basis for manipulation, such as beam combining or beam steering, in which the beams being manipulated (the probe beams) are stronger than the beams creating the grating (the pump beams).[3,4]

The principle of coherent addition of several input laser beams into one output beam has been demonstrated by the use of binary phase gratings.[5] A phase-only (index) grating is desirable to minimize losses; a grating to combine N beams is equivalent to a grating which is designed to produce N orders of equal amplitude from a single incident beam.

Sulfur hexafluoride (SF_6) has been selected as the medium for initial study of beam combining. Calculations show that an index grating can be created by nearly resonant pumping of the ν_4 level of SF_6 with 615.1/cm (16.26 μm) radiation from a CF_4 laser. The radiation to be controlled would be the 10P(16) transition of a CO_2 laser at 947.7/cm (10.55 μm). The pertinent levels and transitions are shown in Figure 1. The calculation of the complex index is done using a nonperturbative method of fields interacting with a multilevel system.[6]

Coupled wave theory[7] has been used to model probe beam interaction with a grating. Computer codes have been written for single beam diffraction by the grating, and for two beam combination.[3,4]

An experimental setup has been assembled for a proof-of-principle demonstration. Since the analytical framework for this study has already been presented,[3,4] this paper concentrates on the experimental effort to date.

2. EXPERIMENTAL SETUP

A simplified schematic of the experimental apparatus is shown in Figure 2.

The pump radiation is provided by a tetrafluoromethane (CF_4) laser which is optically pumped by a CO_2 TEA laser.[8] A low pressure CO_2 laser gain cell inside the TEA laser cavity provides line narrowing for efficient CF_4 pumping. The back mirror of the TEA laser is a 150 lines/mm grating for line select-

ability. Apertures in the TEA cavity ensure TEM_{00} operation. The CF_4 laser has a 152cm cavity length; effective gain length is 122cm terminated by CdTe Brewster windows. Maximum output energy occurs at 3-5 Torr pure CF_4 pressure when the gain cell wall temperature is near 160°K. An aperture at the CF_4 output coupler restricts the CF_4 output to TEM_{00}. Although the CF_4 output coupler has 99.5% reflectance for the CO_2 radiation, a 150 lines/mm grating beyond the output coupler is needed to complete the separation of the CO_2 light from the 16 μm radiation.

In the initial experiments which are reported here, probe radiation came from a conventional line-selectable cw CO_2 laser which was operated in a pulsed mode by pulsing the power supply. The pulse length was about 150 μs, compared to the roughly 50 ns pulse from the CF_4 laser, and was therefore not particularly satisfactory for overlapping pulses in a repeatable manner. Another CO_2 TEA laser is being substituted for the probe laser. Pulse sequencing is now much more reliable.

Both pump and probe radiation are directed to the SF_6 sample cell after beam sampling. A beam splitter can be installed into a beam line so that two beams each may be sent to the sample cell. For each laser individually, the two beam paths are made as equal as possible to insure coherence.

The geometry of the overall experiment gave similar beam sizes of the 16.26 μm pump and the 10.55 μm probe beams in the interaction region of the SF_6 cell. At the SF_6 cell, the gaussian $1/e^2$ diameter of the pump beam was calculated to be 1.16cm; that of the probe beams, 1.23cm. The SF_6 cell is mounted in a rotational mount which has a vernier scale; a HeNe laser defines a reference direction; this combination allows pump and probe beam entrance angles to be set within 0.1 degree. Each pump beam was directed into the cell at 30° from the normal, or 60° apart, so that the interference pattern creates a grating with spacing equal to the pump wavelength. The probe beam(s) are then directed at the Bragg angle predicted by the theory.[3,4]

The SF_6 was contained in a sample cell with 7.5cm diameter KBr windows separated by 1.57cm. SF_6 and a convenient buffer gas could be introduced independently. The buffer gas was necessary to bring the expected low pressure operation of the SF_6 up to a collision-dominated condition. Since KBr is mildly hygroscopic, the cell is normally heated (to about 35-40°C) during exposure to the atmosphere, and kept in a vacuum dessicator when not in use.

Cooled, fast HgCdTe detectors were used (with integrating spheres where necessary) for 10.55 μm detection. At the time the reported experiments were run, the 16.26 μm radiation was detected by pyroelectric energy radiometers; fast detectors have since been received, but were not available for the original work.

3. EXPERIMENTAL RESULTS

Measurements have been made on the transmission of 10.55 μm and 16.26 μm pulses through SF_6.

With the apparatus set up for calculated Bragg angle incidence of 10.55 μm pulses, the path length through the SF_6 was $\sim 1.57/\cos 19^\circ = 1.66$cm. The measured absorption coefficient was $0.16 cm^{-1} Torr^{-1}$ for pressures of 1.6 Torr or below; the value used in the theoretical calculations is $0.4 cm^{-1} Torr^{-1}$. At moderate pressures (4-10 Torr), the transmission of 10.55 μm radiation shows the expected time delays and changes in pulse shape, although the delays seem unusually long.

Data for absorption of 16.26 μm radiation in pure SF_6 are given in Figure 3. The data presented in this and subsequent absorption plots are not normalized (thus the arbitrary ordinate scale); what is plotted for the ordinate variable is a ratio of detector readings, (transmitted sample)/(incident sample). The multimode data appear to be a gentle curve, the single mode data seem to have two slopes, with a break near 12 Torr SF_6 pressure. The absorption below 12 Torr is $0.049 cm^{-1} Torr^{-1}$; above 12 Torr, $0.072 cm^{-1} Torr^{-1}$. The absorption path was 1.81cm since the angle of incidence was 30°. The break in the absorptance at 12 Torr is not understood.

Data for absorption of 16.26 μm radiation in SF_6 in the presence of helium buffer gas are shown in Figure 4. For each data point, the pressure was set by evacuating the cell, admitting SF_6 to its desired pressure, then filling with helium to a total pressure of 18 Torr. Although the data are somewhat scattered (as evidenced by the zero pressure data points), there appears to be only a very slow decrease in transmission until SF_6 pressure is above ~15 Torr, where substantial absorption takes hold. In a variation of the procedure just described, SF_6 pressure was varied again from 0 to 17 Torr, but this time helium was added to give a total pressure ~250 Torr. In the latter experiment, within the data scatter, no 16.26 μm absorptance at all was observed; transmission of 16.26 μm through the cell with 250 Torr of helium (with or without SF_6) was identical to transmission of an empty cell!

A further experiment was run to check the previous surprising result. SF_6 pressure was set at 7.5 Torr and varying amounts of helium were added; the data are given in Figure 5. SF_6 at 7.5 Torr (for our absorptance path) without any helium absorbs about half of the incident 16.26 μm radiation (compare with Figure 3), while addition of helium reduces the 16.26 μm absorption. The break seems to occur at about 2-3 Torr, and this agrees well with the data of Figure 4, in which substantial 16.26 μm absorption occurs only when helium partial pressure has been reduced to less than 2-3 Torr. Thus we see that addition of small amounts of helium into SF_6 gas renders SF_6 partially to totally transparent to 16.26 μm radiation.

Experiments to detect energy at 10.55 μm diffracted from a grating created by the interference of 16.26 μm beams in SF_6 in the presence of helium have been unsuccessful.

4. CONCLUSIONS

Theory shows that the strength of the nonlinear interaction depends on the absorption coefficient of the 16.26 μm radiation as well as the amount of separation (Δ_1 and Δ_2) of the laser radiation from the molecular resonances. The latter, of course, is a quantitative statement of what is "near-resonance." If 16.26 μm absorption disappears, no grating formation can be expected.

The cause of the disappearance of 16.26 μm absorption in SF_6 in the presence of helium buffer gas is not known, but we are prompted to make a reasoned guess. The connection of collisions with spectral line broadening has a long history; careful studies of the effect of foreign gases go back to the 1920s. Mitchell and Zemansky[9] refer to "Lorentz broadening," in which an absorption line can be broadened, have its maximum shifted, and become asymmetric due to collisions with foreign gas molecules. In general, the work reported in the older literature deals with electronic transitions in atomic species, and involve relatively high pressures of buffer gas (hundreds of Torr to atmospheres of pressure). The fact that we are dealing with excited rotational/vibrational transitions of considerably longer wavelength (lower energy transitions) may help to explain the much higher sensitivity to buffer gas pressure that we observe. It may also be observed that we are attempting to pump at 615.1/cm, just to the more energetic side of a Q-branch transition into the ν_4 manifold of SF_6 which has a very sharp cutoff at 615.025/cm.[10] If this transition is shifted to the red by collisions with He, or substantially broadened with lower peak absorption, the effect could be as dramatic as the disapearance of the absorption line that we have observed.

We are currently preparing to repeat the absorption experiments using fast, high sensitivity 16.26 μm detectors. High purity helium, argon, and xenon will each be checked as buffer gases. The SF_6 cell has been reduced to 1mm window separation to allow more pressure flexibility. When the appropriate absorption has been established, the CO_2 TEA probe laser with variable, reliable pulse sequencing will be directed into the interaction region, and diffracted energy sought as proof of grating presence. Parametric studies will be run with pressure, intensity, and angle variation.

5. ACKNOWLEDGEMENTS

This work has been funded by SDIO/IST and managed by the Office of Naval Research under Contract No.

N00014-87-C-0114. The authors are grateful for the contributions of M. O. Gracey in carrying out the experiments.

6. REFERENCES

1. M. Rokni and A. M. Flusberg, "Laser-controlled optics using near-resonance nonlinear dispersion in gaseous media," IEEE J. Quantum Electron. QE-20, 1324-1331 (1984).

2. A. M. Flusberg and M. Rokni, "Bragg reflection by a gain medium optically pumped in a grating geometry," IEEE J. Quantum Electron. QE-22, 730-738, (1986).

3. J. S. Chivian, C. D. Cantrell, W. D. Cotten, and C. A. Glosson, "Beam combining in a gas via nonlinear, diffractive optics," Proc. SPIE 874, 143-150 (1988).

4. C. A. Glosson, C. D. Cantrell, J. S. Chivian, and W. D. Cotten, "Laser beam combining using near-resonance nonlinear dispersion," Paper WM18, Conference on Lasers and Electro-Optics (CLEO '88), 1988 Technical Digest Series, Vol. 7 (Optical Society of America).

5. J. R. Leger, G. J. Swanson, and W. B. Veldkamp, "Coherent laser addition using binary phase gratings," Appl. Opt. 26, 4391-4399 (1987).

6. D. R. Adams, C. D. Cantrell, and W. H. Louisell, "Multilevel, multifrequency laser pulse propagation," Opt. Comm. 43, 292-296 (1982).

7. T. K. Gaylord and M. G. Moharam, "Analysis and applications of optical diffraction by gratings," Proc. IEEE 73, 894-937 (1885).

8. J. J. Tiee and C. Wittig, "CF_4 and NOCl molecular lasers operating in the 16-μm region," Appl. Phys. Letters 30, 420-422 (1977); A. Stein, P. Rabinowitz, and A. Kaldor, "Radiance enhancement of the 16-μm CF_4 laser," Opt. Letters 3, 97-99 (1978); V. Yu. Baranov et al, "Experimental and theoretical investigation of a pulsed laser utilizing the CF_4 molecule," Sov. J. Quantum Electron. 16, 1433-1438 (1986).

9. A. C. G. Mitchell and M. W. Zemansky, Resonance Radiation and Excited Atoms, Ch. 4 (Cambridge, 1961).

10. K. C. Kim, W. B. Person, D. Seitz, and B. J. Kronn, "Analysis of the ν_4 (615 cm^{-1}) Region of the Fourier Transform and Diode Laser Spectra of SF_6," J. Mol. Spectrosc. 76, 322-340 (1979).

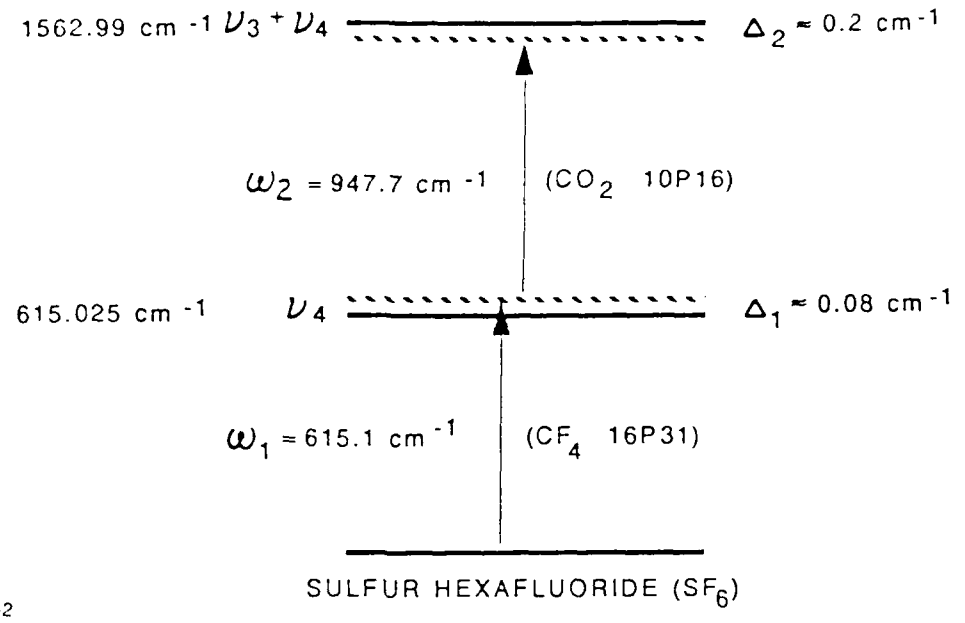

Figure 1. Energy levels and laser lines

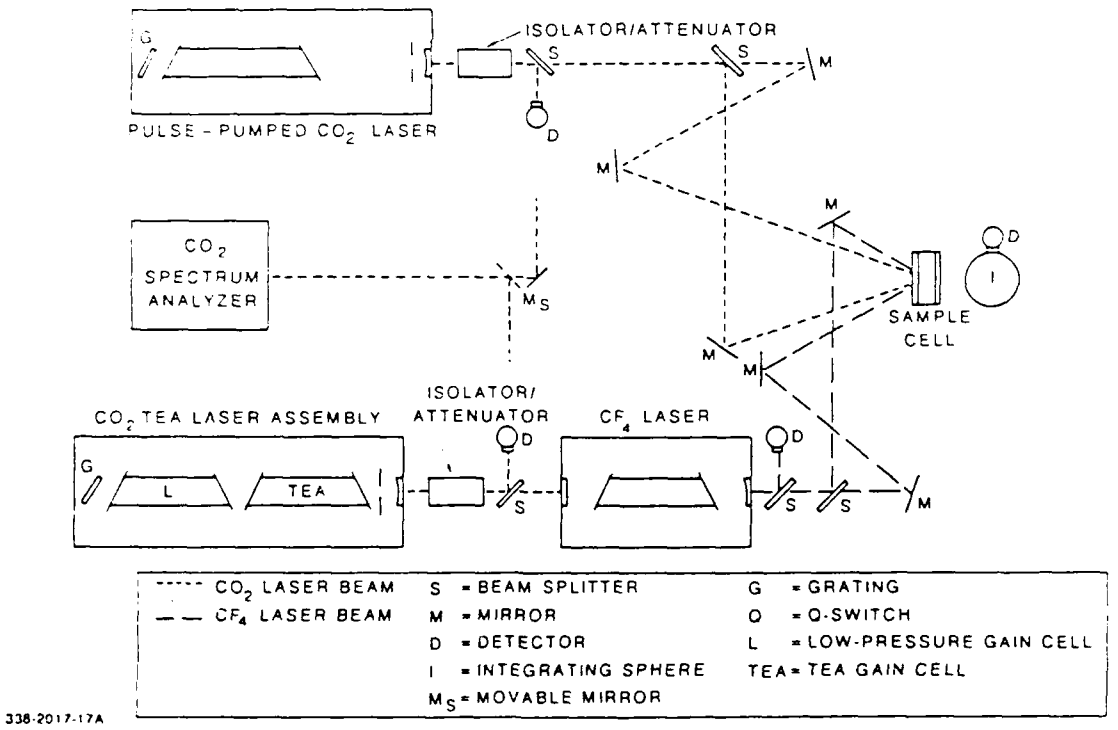

Figure 2. Experimental setup

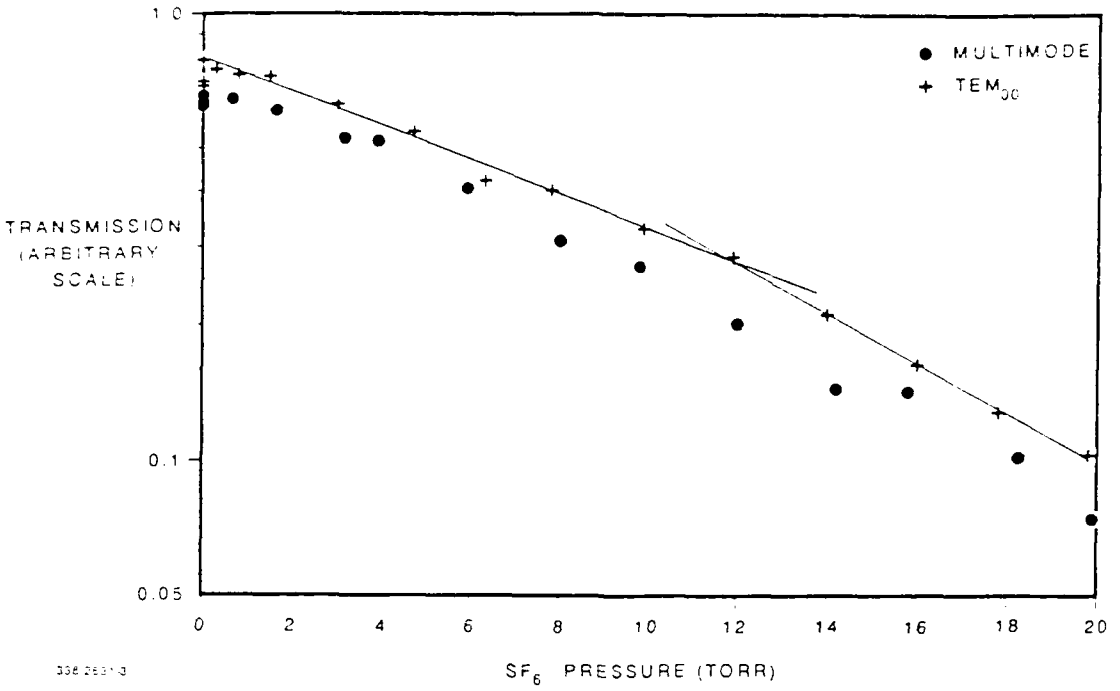

Figure 3. 16.26 μm absorption without helium

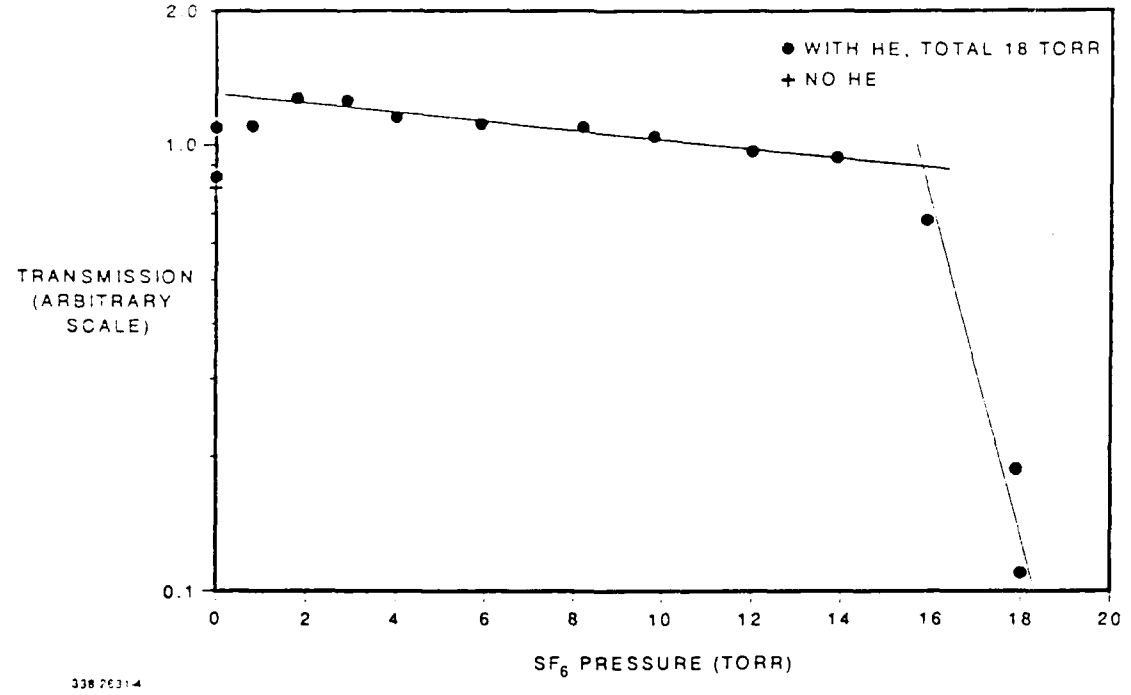

Figure 4. 16.26 μm absorption with helium

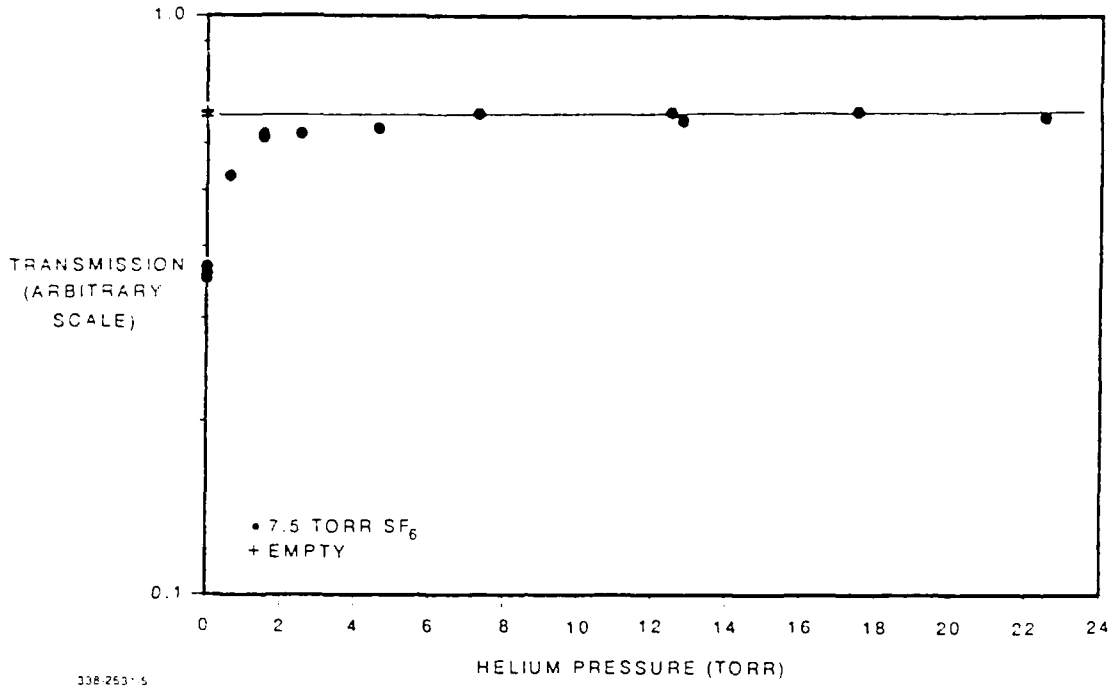

Figure 5. 16.26 μm absorption, fixed SF_6 pressure